Fossil leaf cuticle: Best practices for preparation and paleo-CO2 analysis

Xiaoqing Zhang, Dana Royer, Carina Colombi, Juan Martin Drovandi, Jennifer Mcelwain, Gaëtan Guignard, Qin Leng, Barry Lomax, Nathan Sheldon, Rebekah Stein, et al.

Earth-Science Reviews 264 (2025) 105104

Contents lists available at ScienceDirect

Earth-Science Reviews

journal homepage: www.elsevier.com/locate/earscirev

Fossil leaf cuticle: Best practices for preparation and paleo-CO_2 analysis

Xiaoqing Zhang [a,*], Dana L. Royer [a], Carina E. Colombi [b], Juan Martin Drovandi [b], Jennifer C. McElwain [c], Gaëtan Guignard [d,e], Qin Leng [f], Barry H. Lomax [g], Nathan D. Sheldon [h], Rebekah A. Stein [i], Garland R. Upchurch [j], Yongdong Wang [d], Hong Yang [f,s], Richard S. Barclay [k], Ying Cui [l], Wolfram Kürschner [m], Joseph N. Milligan [k,n], Isabel Montañez [o,p], Jon D. Richey [o,p], Tammo Reichgelt [q], Gongle Shi [d], Selena Y. Smith [h], Margret Steinthorsdottir [r]

[a] Department of Earth and Environmental Sciences, Wesleyan University, Middletown 06459, USA
[b] Instituto y Museo de Ciencias Naturales, Universidad Nacional de San Juan - CIGEOBIO, CONICET, Av. España 400 (N), J5400DNQ, San Juan, Argentina
[c] School of Natural Sciences, Botany, Trinity College Dublin, College Green, Ireland
[d] State Key Laboratory of Palaeobiology and Stratigraphy, Nanjing Institute of Geology and Palaeontology and Center for Excellence in Life and Palaeoenvironment, Chinese Academy of Sciences, Nanjing 210008, China
[e] Université Claude Bernard Lyon 1, LEHNA UMR 5023, CNRS, ENTPE, F-69622 Villeurbanne, France
[f] Laboratory for Terrestrial Environments, Department of Biological and Biomedical Sciences, Bryant University, Smithfield, RI 02917, USA
[g] School of Bioscience, University of Nottingham, Sutton Bonington Campus, Loughborough LE12 5RD, UK
[h] Department of Earth and Environmental Sciences, University of Michigan, Ann Arbor, MI 48109, USA
[i] Cooperative Programs for the Advancement of Earth System Science, University Corporation for Atmospheric Research, Boulder, CO 80301, USA
[j] University of Colorado Museum of Natural History, Boulder, CO 80309, USA
[k] Department of Paleobiology, National Museum of Natural History, Smithsonian Institution, 1000 Madison Dr. NW, Washington DC 20560, USA
[l] Department of Earth and Environmental Studies, College of Science and Mathematics, Montclair State University, Montclair, NJ 07043, USA
[m] Natural History Museum and Department of Geoscience, University of Oslo, Oslo 0162, Norway
[n] Department of Environmental Science and Studies, Washington College, 300 Washington Ave., Chestertown, MD 21620, USA
[o] University of California, Davis Institute of the Environment, University of California, 1 Shields Avenue, Davis, CA 95616, USA
[p] Department of Earth and Planetary Sciences, 1 Shields Avenue, Davis, CA 95616, USA
[q] Department of Earth Sciences, University of Connecticut, 354 Mansfield Rd, Storrs, CT 06269, USA
[r] Department of Bioinformatics and Genetics, Swedish Museum of Natural History, 114 18, Stockholm, Sweden
[s] Department of Earth and Planetary Sciences, Harvard University, Cambridge, MA 02138, USA

ARTICLE INFO

Keywords:
Paleobotany
PALEOCLIMATE
Leaf cuticle
Stomata
Leaf-gas exchange
Stable Isotopes

ABSTRACT

Leaf cuticle is the waxy envelope that protects leaves from desiccation, UV damage, and abrasion. The cuticle encodes information about a plant's chemistry and leaf epidermal and stomatal cell morphology. Fossil leaf cuticle has been used to determine taxonomic affinities for almost two centuries and recognized in recent decades for its value in reconstructing paleoenvironments and paleoclimates, especially atmospheric CO_2. Fossil leaf cuticle preparation techniques are typically reported as single workflows tied to individual studies, starting with finding fossils in the field through the steps of preparing cuticle for chemical and morphological analysis, including decisions about type of microscopy and level of sampling effort at different spatial scales (number of fields-of-view, leaves, and species). The siloed nature of these publications makes finding appropriate methods and workflows for new studies difficult, especially for less experienced researchers. Here, we attempt to synthesize a breadth of existing workflows and make recommendations to guide methodological decision-making for new studies, with a particular focus on paleo-CO_2 reconstruction via a proxy based on leaf gas-exchange principles (the Franks model). We describe and annotate chemical procedures for preparing cuticles for analysis and include recommendations regarding leaf conditions for which each is most appropriate. For studies making repeated measures of morphology (e.g., stomatal density), we describe a resampling routine that can guide decision-making, in real time, about sampling effort.

* Corresponding author.
E-mail address: xzhang04@wesleyan.edu (X. Zhang).

https://doi.org/10.1016/j.earscirev.2025.105104
Received 7 January 2025; Received in revised form 7 March 2025; Accepted 13 March 2025
Available online 19 March 2025

Contents

1. Introduction

The emergence of leaf cuticle represents a pivotal evolutionary innovation that enabled plants to colonize terrestrial ecosystems. The cuticle is an extra-cellular, hydrophobic layer consisting primarily of cutin and cuticular waxes that covers the outer surface of the epidermis and serves as a protective layer against water loss, insect attack, and UV radiation (Esau, 1977; Kolattukudy, 1980; Kolattukudy, 1987; Kolattukudy and Espelie, 1989; Jeffree, 1996; Rozema et al., 1997; Laakso et al., 2000; Bruhn et al., 2014; Bernado et al., 2021; Sánchez et al., 2021; Moreno et al., 2022; Jolliffe et al., 2023; Molina et al., 2023; Heredia et al., 2024). The cuticle forms a natural cast of the underlying epidermis and reflects its characteristic features, including epidermal pavement cells, stomatal patterns, trichomes, glands, and papillae. Fossil cuticles present similar features to extant cuticles, including waxy appearance, morphology of the stomatal apparatus (Barthel, 1962; Cleal and Zodrow, 1989; Psenicka et al., 2005; Zodrow and Mastalerz, 2007), and biopolymeric composition, i.e., cutin or cutan (Holloway, 1982; van Bergen et al., 1994; Lyons et al., 1995; Zodrow and Mastalerz, 2001; van Bergen et al., 2004; de Leeuw et al., 2006; Zodrow and Mastalerz, 2009; Zodrow, 2021).

1.1. Why is fossil cuticle important?

1.1.1. Morphology

Fossil leaf cuticles were first described in the 19th century (Brongniart, 1837; Göppert, 1841; Brodie, 1842; Unger, 1852) and ever since have been widely used for systematic research (for overview, see Zodrow and Mastalerz, 2009). In particular, epidermal cell shapes and orientations, the structure of the stomatal complex, and the presence of specialized structures like trichomes, glands, striations and papillae, can be used to taxonomically classify fossil plants (Florin, 1951; Florin, 1958; Stace, 1965b; Stace, 1965a; Stace, 1966; Dilcher, 1974; Metcalfe and Chalk, 1979; Cutler, 1982; Stace, 1984; Kerp, 1990; Barale and Baldoni, 1993; Maheshwari and Bajpai, 1996; Kürschner, 1997; Barclay et al., 2007; Martínez et al., 2020; Drovandi et al., 2022).

Because leaf cuticle is the critical boundary between plants and the environment, aspects of cuticle can reflect the environmental and ecological conditions the plant is growing in (Archangelsky et al., 1995; McElwain and Chaloner, 1996; Matthaeus et al., 2023; McElwain et al., 2024). For example, features on the leaf cuticle, such as stomatal size and density, change with atmospheric CO_2 and can thus be used to reconstruct the paleo-CO_2 concentration (for reviews, see Royer, 2001; Jordan, 2011; McElwain and Steinthorsdottir, 2017). Leaf morphological features encoded in cuticle also reflect genome size (Cavalier-Smith,

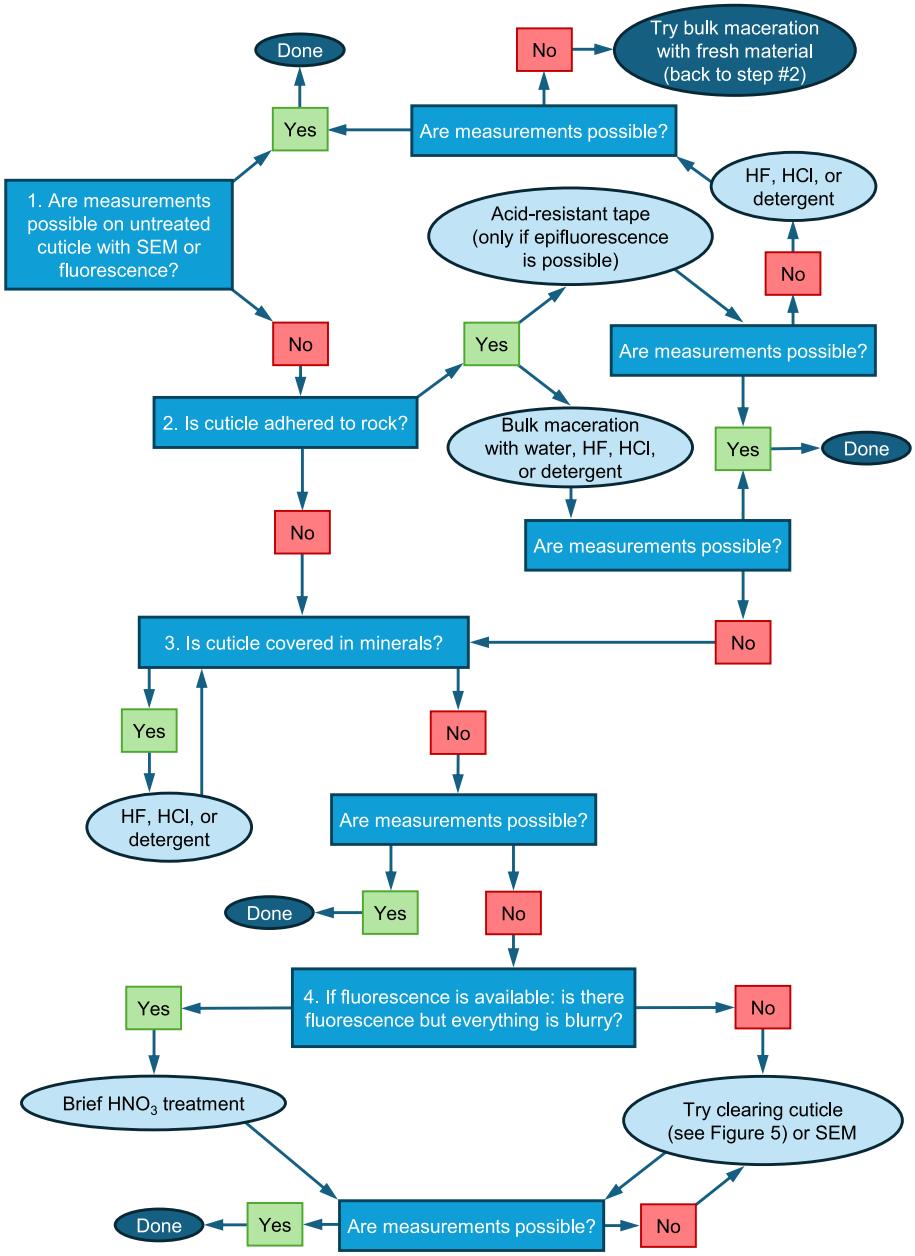

Fig. 1. Workflow for preparing fossil leaves for observation of cuticle under a microscope (see Sections 3.1–3.2).

2005; Beaulieu et al., 2008; Veselý et al., 2012; Lomax et al., 2014; McElwain and Steinthorsdottir, 2017; Roddy et al., 2020; Faizullah et al., 2021; Bhadra et al., 2023) and light environment (Jordan et al., 2014; Bush et al., 2017; Milligan et al., 2021; Poorter et al., 2025).

1.1.2. *Chemistry*

Chemical analyses of fossil cuticle—especially gas chromatography (GC)—can be taxonomically informative (Mösle et al., 1997; Mösle et al., 1998; Nguyen Tu et al., 2003; Colombi et al., 2011; D'Angelo and Zodrow, 2011; Zodrow et al., 2012; D'Angelo and Zodrow, 2018; D'Angelo, 2019; D'Angelo and Zodrow, 2022; D'Angelo, 2023; Matthaeus et al., 2023; D'Angelo et al., 2024b). Additionally, plant cuticle $\delta^{13}C$ values provide information about photosynthetic pathways, i.e., C_3, C_4, or CAM photosynthesis (Tipple and Pagani, 2007; Zahajská et al., 2024); physiological status in relation to irradiance, temperature, nutrient supply, water stress, and salt stress (Farquhar et al., 1980; Farquhar and Sharkey, 1982; Guy and Reid, 1986; Tieszen, 1991; Nguyen Tu et al., 1999; Arens and Jahren, 2000; Arens et al., 2000; Diefendorf et al., 2010; Kohn, 2010; Colombi et al., 2011; Sheldon et al., 2020; White et al., 2020; Richey et al., 2021; Stein et al., 2021a; Matthaeus et al., 2023; McElwain et al., 2024; Zahajská et al., 2024); light environment and canopy-level of the leaf (Graham et al., 2014; Graham et al., 2019); and atmospheric CO_2 concentration (Schubert and Jahren, 2012). Notably, $\delta^{13}C$ values in leaves are influenced by the ratio of internal CO_2 to atmospheric CO_2 (Farquhar et al., 1989; Schubert and Jahren, 2012; Cui and Schubert, 2018), but the expected inverse correlation between atmospheric CO_2 concentration and $\delta^{13}C$ values is absent in many species (Kohn, 2010; Stein et al., 2019; Sheldon et al., 2020; Stein et al., 2021b; Scher et al., 2022).

$\delta^{15}N$ values from cuticles convey information about associations with nitrogen fixing symbionts (Kipp et al., 2024) and may additionally be related to temperature, precipitation, and soil nitrogen availability (Craine et al., 2009). The C/N can help distinguish between taxonomic groups (Matthaeus et al., 2023), aerobic and anaerobic decay (Colombi et al., 2011), and may for some taxa be weakly related to climatic factors such as temperature and precipitation (Stein et al., 2019; Sheldon et al.,

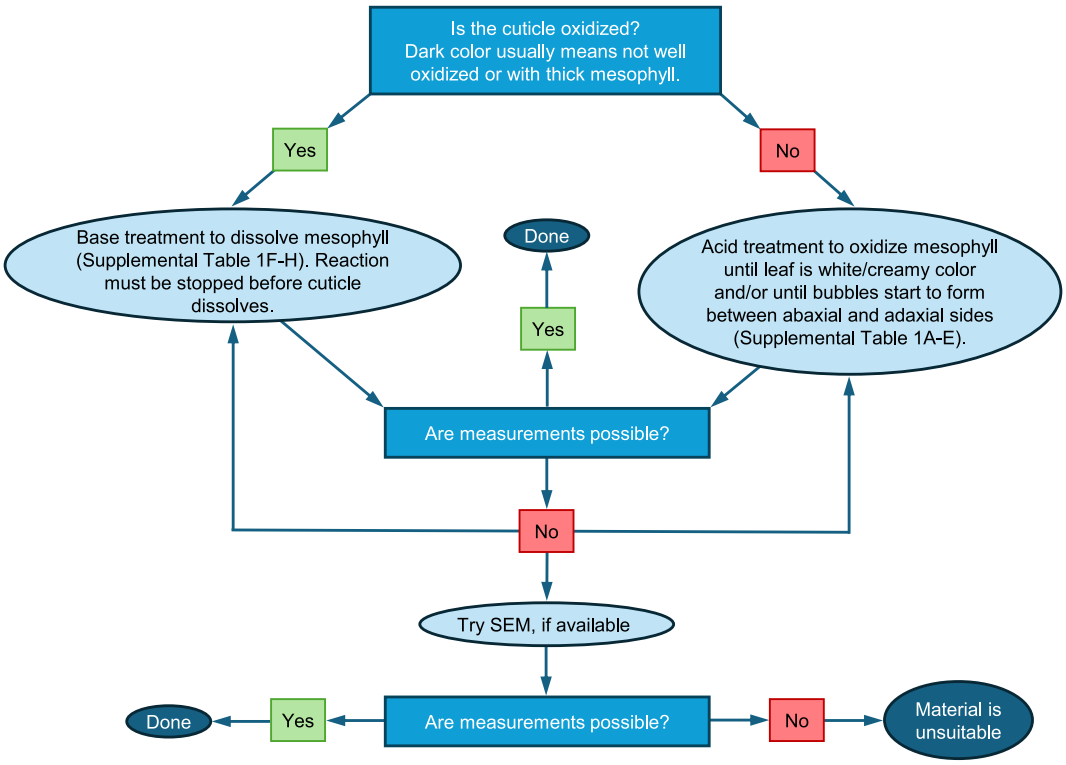

Fig. 2. Workflow for clearing and cleaning fossil leaves so that the cuticle is translucent (see Section 3.3).

2020; Stein et al., 2021a) or used as a paleo-functional trait (Matthaeus et al., 2023; McElwain et al., 2024).

1.2. *Why is an overview of fossil cuticle preparation and analysis needed?*

Compiled methods for the preparation of fossil cuticles are decades old (Upchurch, 1995; Kerp and Krings, 1999; Sun et al., 2009). Since then, new preparatory methods (e.g., Barclay et al., 2010), new analytical methods such as FTIR (e.g., Zodrow et al., 2009), and applications (Franks et al., 2014; Konrad et al., 2017) have been developed and published, highlighting the need for a new synthesis of "best practices". We intend this synthesis to be a reference point for all common leaf cuticle preparation practices, as well as provide inspiration for those looking to incorporate new techniques into their scientific methods.

2. Preservation of plant fossils

Fossil plants are preserved in a variety of depositional environments, from shallow marine to continental basins (Supplementary Table 1 in Supplemental material 1; Wing, 1988; Behrensmeyer and Hook, 1992). Their preservation is a function of allogenic (mainly climate and tectonism) and authigenic factors (e.g., degree of water saturation, grain size of the host sediments, sudden devastating events that transport and deposit vegetation en masse, such as storms, floods, fires, ashfalls, and pyroclastic flows; Gastaldo and Demko, 2011; Kumar et al., 2015) that modify the accommodation space and sedimentation rate of a depocenter (e.g., Holz and Simões, 2005; Gastaldo and Demko, 2011; Colombi et al., 2017).

In coastal subaqueous marine settings, such as estuaries, lagoons, inner platforms, and tidal areas, plant remains have a high potential to be buried because erosion rates are relatively low (Behrensmeyer and Hook, 1992). In marginal to nearshore marine environments, plant cuticles are preserved in argillaceous organic-rich sandstones (Barclay, 2011). Additionally, cuticles have been identified in carbonate concretions in shales from outer continental shelf to upper continental slope environments, as well as in deep-water organic mudstones (Upchurch, 1984; Upchurch, 1995; Richey et al., 2023).

Among continental settings, alluvial and lacustrine deposits commonly preserve fossil plants. Dispersed plant cuticles occur in a range of terrestrial sedimentary rocks, including coal, argillaceous sandstones, carbonaceous shales, mudstones, and siltstones (Barclay, 2011). Standing bodies of water—such as lakes, ponds, marshes, abandoned channels, and swamps—have the highest potential for fossil preservation due to their permanently water-saturated sediment bottoms (Spicer, 1989). These confined environments promote plant preservation due to several factors: limited oxygen, sediment accumulation that isolates organic remains from oxygen and microbes, slow water circulation that further limits oxygen availability, favorable chemical conditions for preservative compounds, and stable temperatures that inhibit decomposer activity (Gastaldo and Huc, 1992; Gastaldo and Demko, 2011).

Volcaniclastic deposits also provide exceptional preservation environments. Rapid burial in ash preserves plant habitats that are otherwise underrepresented in the sedimentary record (Spicer, 1991; Behrensmeyer and Hook, 1992; Wing et al., 1993; Cúneo et al., 2003; Wang et al., 2012). Ash that blankets landscapes enhances preservation by adhering to leaves, either melting waxes or sticking to moisture, causing leaf abscission and rapid burial in the ash (Spicer, 1991). Additionally, volcaniclastic material can alter sediment and pore-water chemistry, increasing mineralizing fluids and promoting early diagenesis, such as sulfide precipitation (Burnham and Spicer, 1986; Spicer, 1991; Diaz et al., 2018).

Other exceptional sites for plant preservation include tar seeps (Miller, 1983; Marcus and Berger, 1984), karst fissure fills (O'Leary, 1981), tree hollows (Walton, 1935), feces and regurgitated matter (Fisher, 1981; Andrews, 1990), plant packrat middens (Van Devender et al., 1987; Hall, 1988), maar deposits (Uhl et al., 2024), and freshwater springs (Rolfe et al., 1990).

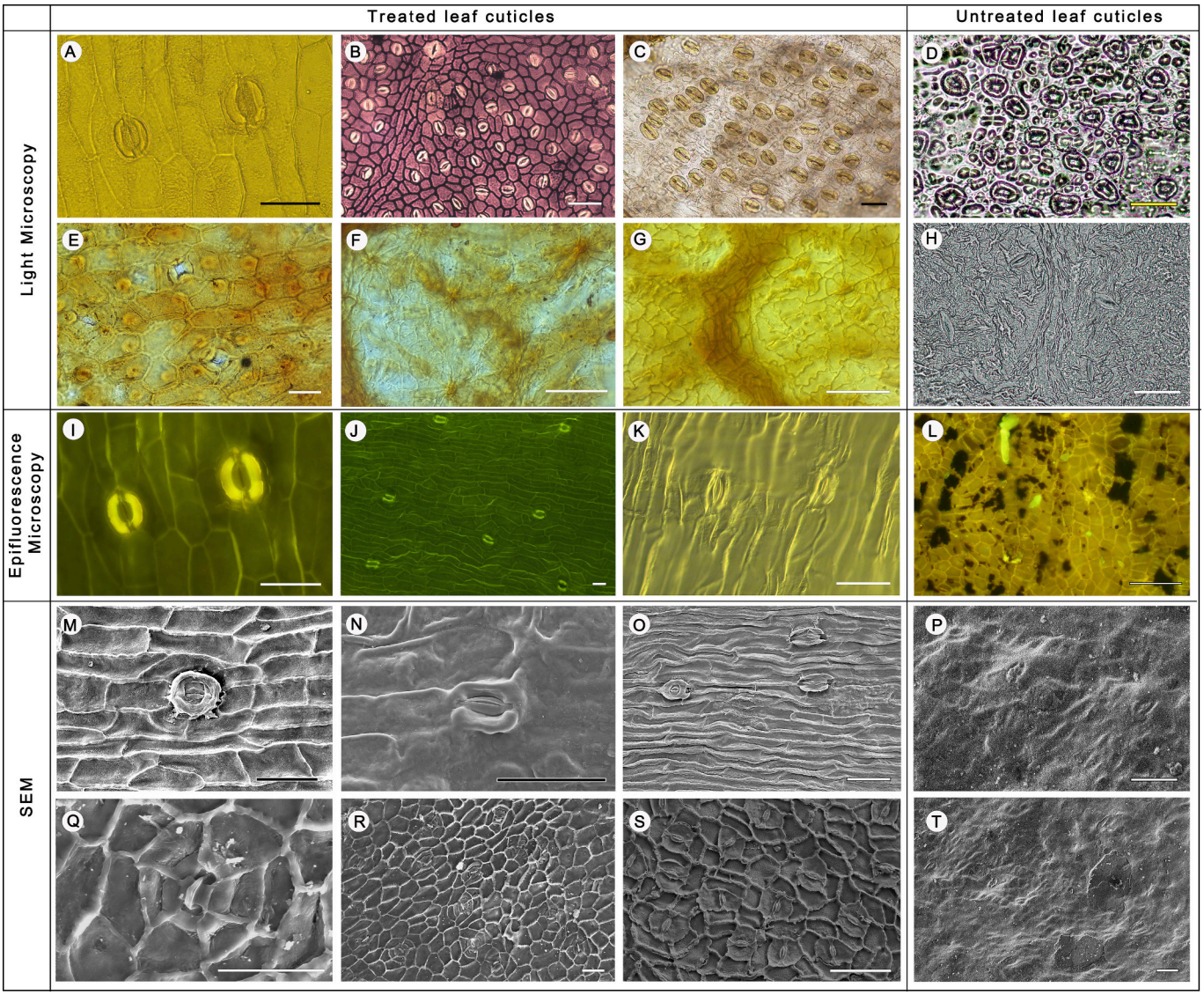

Fig. 3. Leaf cuticle images under different microscopy. (A) Cleared leaf cuticle of Cretaceous *Pseudotorellia resinosa* Shi, Herrera, Herendeen, Leslie, Ichinnorov, Takahashi & Crane under light microscopy (Zhang et al., 2024). (B) Cleared leaf cuticle of Oligocene/Miocene *Litsea calicarioides* (A.Cunn.) Benth. & Hook.f. ex Kirk under light microscopy (Reichgelt et al., 2016); C) Cleared leaf cuticle of extant *Thuja occidentalis* Linnaeus. (D) Dental putty mold of uncleared extant leaf cuticle of *T. occidentalis* under light microscopy. (E) Cleared leaf cuticle of Triassic *Dicroidium* (*Zuberia*) *zuberi* (Szajnocha) Archangelsky under light microscopy (Drovandi et al., 2022). (F, G) Sun and shade leaf, respectively, of Neogene *Quercus pseudocastanea* Goeppert under light microscopy (Kürschner, 1997). (H) Dental putty mold of uncleared leaf cuticle of extant *Populus tremuloides* Michaux under light microscopy. (I, J) Cleared leaf cuticle of Cretaceous *Pseudotorellia resinosa* under epifluorescence microscopy; the field-of-view in panel I is identical to that in panel A. (K) Cleared leaf cuticle of Cretaceous *Pseudotorellia palustris* Shi, Herrera, Herendeen, Leslie, Ichinnorov, Takahashi & Crane under epifluorescence microscopy. (L) Untreated fruit wing cuticle of Cretaceous *Wireroadia viccallii* Zhang, Wang, Dilcher & Manchester (Zhang et al., 2020). (M) Inner surface of treated leaf cuticle of Cretaceous *Pseudotorellia resinosa* under SEM (Shi et al., 2018). (N) Outer surface of treated leaf cuticle of Cretaceous *P. resinosa* under SEM (Shi et al., 2018). (O) Inner surface of treated leaf cuticle of Cretaceous *P. palustris* under SEM (Shi et al., 2018). (P, T) Untreated wing cuticle of Cretaceous *Wirerodia major* (Hollick) Zhang, Wang, Dilcher & Manchester under SEM (Zhang et al., 2020). (Q, R) Cleared leaf cuticle of Triassic *Dicroidium (Zuberia) zuberi* under SEM (Drovandi et al., 2022). (S) Cleared leaf cuticle of Oligocene *Laurophyllum gengjiaoae* Shi, Xie & Li under SEM (Shi et al., 2014). All scale bars = 50 μm.

3. Fossil leaf cuticle preparation

Multiple steps are normally needed to prepare fossil leaf cuticle for microscopy and/or further chemical analyses. These steps are usually informed by some key themes: (1) determining if cuticle is present (Section 3.1); (2) determining how to isolate the fossil from its rock matrix (Section 3.2); and (3) determining how to best "clear" (transparent/translucent whole leaf with mesophyll tissue, epidermises, and cuticular membranes all remained) and/or "clean" (only the cuticular membrane, mesophyll tissue has been removed) a fossil plant so that it is transparent to visible light (Section 3.3). Navigating these steps can be difficult because although many workflows exist in the literature, the best workflow for any given study can depend highly on taxonomy, sedimentary setting, fossil preservation, and study goals. For instance, some cuticle preparation procedures that yield excellent results for observing stomatal traits needed for paleo-CO_2 proxies can alter the cuticle chemical composition (i.e., $\delta^{13}C$) (see Section 6.1.3), which is an input parameter for CO_2 proxy models (see Section 5). Here we try to synthesize these workflows (Figs. 1–2) and provide some general recommendations.

3.1. Does my fossil contain cuticle?

Leaf compression fossils can consist entirely of cuticle with little-to-no coalified mesophyll or they can contain substantial mesophyll tissue in varying states of preservation, thermal alteration, and degrees of coalification, with or without a preserved cuticular envelope. The former fossils typically appear yellow to brown in colour on the rock and the latter black. To determine if a leaf fossil contains cuticle, a convenient approach is to view it under a microscope with a UV light source because phenolic compounds within cuticle strongly autofluorescence in the blue (435–500 nm), cyan (500–520 nm), and sometimes green (520–565 nm) wavelengths of light (Moreno et al., 2022; Moreno et al., 2023). Mesophyll tissue, in contrast, does not fluoresce under UV light. Epifluorescence microscopy can be used on compression fossils and dispersed cuticle fragments that are still attached to their rock matrix. In some cases, all measurements (stomatal density, cell size, etc.) can be made at this stage, eliminating the need for destructive chemical treatments (see "yes" to Question 1 in Fig. 1).

However, fossil cuticle autofluorescence can be weak or entirely absent even if cellular details on the cuticle are present. In these cases, the best ways to identify the presence of cuticle are to observe the fossil in question under SEM or to clear any mesophyll (Fig. 2; see also Supplemental Table 2 in Supplemental material 1 for clearing methods), stain if necessary, and then view under transmitted light.

3.2. Release of fossil leaf and cuticle fragments from rock matrix

For fossils that autofluoresce but the host rock is too large or thick to fit under a microscope, acid-resistant tapes, such as cellulose acetate peels and polyester overlays, are effective for separating cuticle from rock (Kouwenberg et al., 2007). The stripped cuticle can be further treated with acids to remove remnant silicates, carbonates, etc. (see "acid-resistant tape" in Fig. 1). This technique is especially appropriate for leaves with a "cracked" texture that under normal maceration (without tape) would disaggregate into many pieces, destroying their original orientation. A drawback is that only one side can be viewed under a microscope (the side not adhered to the tape).

At this stage, for fossils where epifluorescence will not work (either because the image quality is not sufficient or because an appropriate microscope is not available), they must first be released from the rock matrix via a process called bulk maceration ("yes" to Questions 2 or 3 in Fig. 1). Because cuticle is chemically resistant, bulk maceration aims to dissolve and/or disaggregate mineral material comprising the sediment. Hydrochloric acid (HCl) dissolves carbonates, hydrofluoric acid (HF) dissolves silica, and strong detergent (e.g., Sparkleen™, sodium hexametaphosphate [i.e., Calgon®], sodium pyrophosphate), hydrogen peroxide (H_2O_2), and sometimes even pure water for weakly lithified rock, deflocculates clay particles.

With macrofossils, loosely attached cuticle can sometimes be removed directly with tweezers. If this is not feasible, appropriate macerating chemicals need to be applied. The goal here is to dissolve enough rock so that the cuticle can be lifted off the matrix. This can be done by: (1) applying the appropriate chemical directly on the sediment surface; (2) chipping smaller pieces of leaf (with attached rock) and submerging the pieces in the chemical; or (3) submerging the entire specimen in the chemical (e.g., Upchurch, 1995; Maxbauer et al., 2014; Kowalczyk et al., 2018).

For mesofossils (mm-scale fossils and fossil fragments present throughout the rock volume), the rate at which maceration yields clean cuticle pieces is dependent on the concentration of chemical used, the surface area to volume ratio of the rock matrix, and the degree of induration of the host rock. Small fragments of rock (~1–2 cm^3), for example, have fast reaction times whereas large hand specimens (~5 to 15 cm^3) with whole macrofossils have slower reaction times. The more indurated the rock, the slower the reaction, though rocks with a high calcium carbonate content will process quickly regardless. Also, the higher the concentration of chemical used, the faster the reaction times. The bulk maceration protocol of Wellman and Axe (1999)—modified by Barclay et al. (2010) and Fay (2014)—has been successful in yielding Cretaceous fossil cuticles from sedimentary rock samples with little obvious macrofossil leaf material present (Supplemental Table 3 in Supplementary material 1) and can be further adjusted as required.

After bulk maceration, sometimes measurements are possible under epifluorescence. If autofluorescence is strong but the field-of-view is blurry, a very brief (seconds to minutes) nitric acid (HNO_3) treatment can help by removing any overlying organic films (Upchurch, 1995; Maxbauer et al., 2014) ("yes" to question 4 in Fig. 1). If measurements are still not possible, an environmental SEM can be attempted; failing that, the fossil mesophyll must be cleared and/or removed (Section 3.3; Fig. 2).

3.3. Clearing and cleaning of fossil leaf cuticle for microscopy

Following bulk maceration (Section 3.2), the extracted and sorted fossil cuticle can range from opaque to translucent. Some level of translucency is required to observe stomatal traits using conventional transmitted light microscopy. Typically, for a successful preparation, a combination of acids and bases are needed (Fig. 2; Supplemental Table 2 in Supplementary material 1), which are effective for clarifying (clearing) and dissolving (cleaning) mesophyll tissue, respectively (Liang et al., 2022a; Liang et al., 2022b).

After chemical treatment, if possible, the upper (adaxial) and lower (abaxial) epidermises can be separated using the leaf margin as a hinge. An acupuncture pin, fine dissecting needle, or single paintbrush bristle works well, in combination with the bulb end of another pin to hold down the cuticle. Once separated, use a small paint brush with a few soft bristles and rinse frequently with water to remove any leftover mesophyll and veins. If the goal of the project is to measure aspects of the stomatal complex, it is usually better to view the interior side of the epidermis (e.g., Barclay and Wing, 2016, Fig. 3M-N), especially if the stomata are sunken.

All chemical treatments should be undertaken with care because they can degrade cuticular topographic and anatomical features (e.g., guard cell geometry). For example, if the treatment is too vigorous or runs for too long, the cuticle can break apart or become so thin that micromorphological details are lost. Thus, each step requires careful and continuous monitoring under a microscope. After each chemical step, samples should be rinsed three or more times in deionized water to halt the reaction.

Because fossils are not always abundant, we recommend starting with the weakest base treatment (e.g., diluted commercial bleach). If there is no clear reaction, try an acid treatment to oxidize the mesophyll until the leaf is white/creamy colour or until bubbles start to form between abaxial and adaxial sides. We suggest starting with moderate acids (e.g., Supplemental Table 2 A-D in Supplementary material 1). Stronger acids (e.g., Schultz's Solution, Supplemental Table 2E in Supplementary material 1) should only be used as a last resort.

In the case of middle Miocene conifers, Liang et al. (2022a, 2022b) present an example of an integrated approach. They found 5 % potassium hydroxide (KOH) and 70 % nitric acid (HNO_3) to be the most effective treatment for clearing, followed by some dissolution of the remaining mesophyll with dilute (0.4 %) bleach so that the two epidermises could be separated. The bleach step needs to be carefully monitored because eventually it will also dissolve the thicker cell walls of the epidermis unless clean cuticles rather than cleared leaf epidermises (CLE, refer to Liang et al., 2022b) are desired.

3.4. Staining and mounting prepared cuticle for light and epifluorescence microscopy

The most common histological stains used on fossil plant cuticles are Crystal Violet ($C_{25}N_3H_{30}Cl$), Safranin O ($C_{20}H_{19}ClN_4$), Toluidine Blue

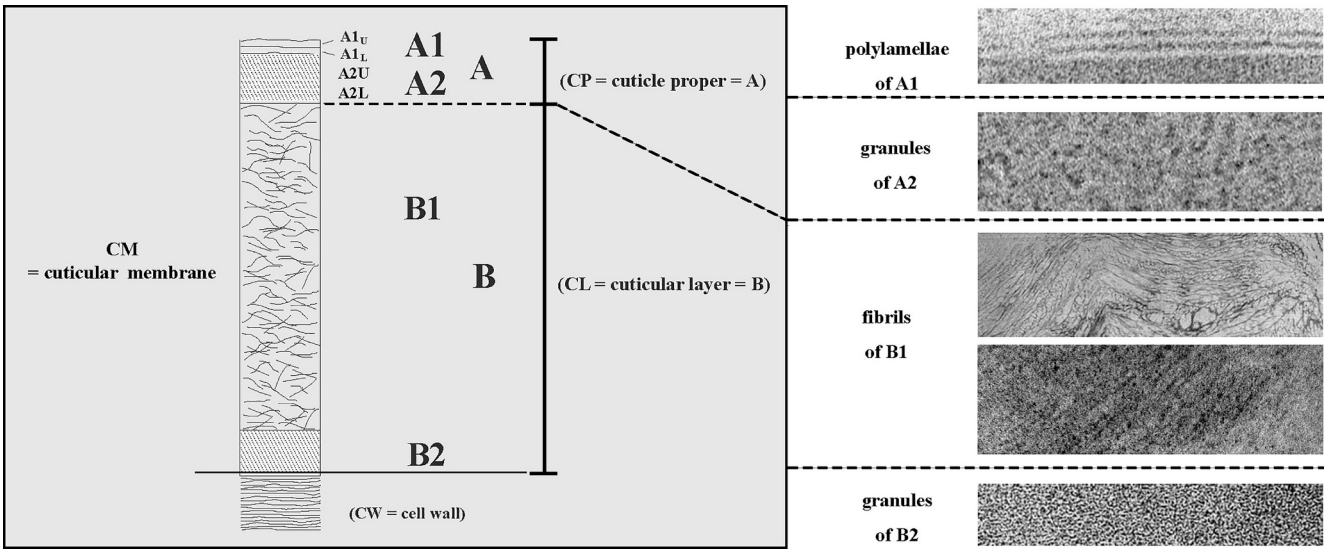

Fig. 4. The synthetic cuticle ultrastructure layer and sublayer terminology (after Guignard (2019); modified according to Archangelsky and Taylor (1986), Holloway (1982), Guignard and Zhou (2005), Nosova et al. (2016) and Guignard et al. (2024)).

($C_{15}H_{16}ClN_3S{\cdot}0.5ZnCl_2$), and Bismark Brown ($C_{18}H_{18}N_8 \cdot 2HCl$). However, staining is not always necessary. Photographing cuticles without staining using differential interference contrast (DIC), phase contrast or epifluorescence microscopy often yields excellent images.

For temporary slides, use a drop of glycerine, then optionally seal under a cover slip with nail polish (nitrocellulose polymer) (Zhang et al., 2024). Alternatively, a temporary water mount may be sufficient; in this case, cuticles should be stored in vials after use either dry or in weakly acidified water (5 % HCl). For permanent slides using transmitted light microscopy, Canada balsam works well and can last for more than 150 years (Ravikumar et al., 2014). Canada balsam (and some other natural resins) autofluoresces, rendering them inappropriate for epifluorescence. Non-fluorescing alternatives include glycerine jelly and synthetic resins like DePeX, Histomount, Coverbond, and Eukitt, but these are prone to oxidation and decay (e.g., several decades for glycerine jelly sealed with nail polish, <10 years for Coverbond in our experience). The components of synthetic resins are proprietary and therefore hard to ascertain. Thus, for fossils where epifluorescence microscopy is expected, we recommend temporary water mounts and permanent storage in vials.

No stains or mounting media should be used on cleared fossil leaves or clean cuticles that will be used in $\delta^{13}C$ analysis, as these media can interfere with the original isotopic signal (Barral et al., 2015).

3.5. *Mounting cuticle for scanning electron microscopy (SEM)*

Leaf cuticles can be mounted for SEM without prior treatment. An advantage of clean cuticle over unclean (either cleared or not) is that the inner surface can be mounted facing up. Although leaf cuticle is predominantly comprised of carbon, applying a layer of gold sputter coating to prevent charging improves the signal-to-noise ratio and enhances the overall quality of the images.

4. Observing cuticle at high magnification

4.1. *Transmitted light microscopy*

For fossil cuticles whose mesophyll has been cleared and/or cleaned, observation under transmitted light microscopy is preferable. Both Differential Interference Contrast (DIC) and *Z*-Stacking using a stacked image capture and analysis system helps to bring into focus the 3D surface of the cuticle (stomatal pores, guard cells, etc.; Fig. 3A-C, E-G).

Micron-scale leaf impression methods developed for living plants (Weyers and Johansen, 1985; Lake and Woodward, 2008) using silicon-based dental putty (e.g., Martin et al., 1991; Gitz and Baker, 2009) can also be applied to fossil plants (Matthaeus et al., 2020; Stein et al., 2024). A cast of these impressions can be made with quick-dry nitrocellulose (i.e., nail polish), then peeled off with tape and viewed under transmitted light microscopy (Slavík, 1974; Martin et al., 1991; Wu and Zhao, 2017; Stein et al., 2024; Fig. 3D, H).

4.2. *Epifluorescence microscopy*

4.2.1. *Epifluorescence observation on cleaned leaves*

For plants with sunken and highly ornamented guard cells, including thickened subsidiary cells or papillae, guard cell length and width in cleaned leaves can be harder to measure under transmitted light than epifluorescence (e.g., Montañez et al., 2016; Richey et al., 2021; Liang et al., 2022a; Liang et al., 2022b; Zhang et al., 2024). In this case, cleaned leaves under epifluorescence light may give a better view (Fig. 3I-K). For example, the Late Triassic– Early Cretaceous Ginkgoalean *Pseudotorellia resinosa* Shi, Herrera, Herendeen, Leslie, Ichinnorov, Takahashi & Crane possesses thickened subsidiary cells that partly overlap the underlying guard cells (Shi et al., 2018; see their fig. 16C-E). These thickened areas are prominent under both transmitted light (Fig. 3A) and epifluorescence (Fig. 3I) and comprise a smaller footprint than the underlying guard cells. The overlapping thickened subsidiary cells may obscure the edges of guard cells unclear under transmitted light (Fig. 3A).

4.2.2. *Epifluorescence observation on uncleared leaves*

Epifluorescence microscopy is particularly useful for fossils where destructive sampling is unwise or forbidden, such as type specimens (Zhang et al., 2020, Fig. 3L), so long as care is taken to minimize exposure to the UV light, which can cause fluorescence quenching (loss of cellular detail). However, image quality from epifluorescence can vary greatly depending on, among other aspects, plant taxonomy and burial history. Different filter cubes can sometimes enhance the intensity of fluorescence (see Section 3.1), as can working in a dark room at full bulb brightness with all light directed to the eyepiece or camera. Brief HNO_3 treatment applied directly to sample surfaces may additionally enhance image quality (see Section 3.2 and Fig. 1 question 4). However, cellular detail is often best captured using transmitted light microscopy with cleared cuticle rather than epifluorescence microscopy with

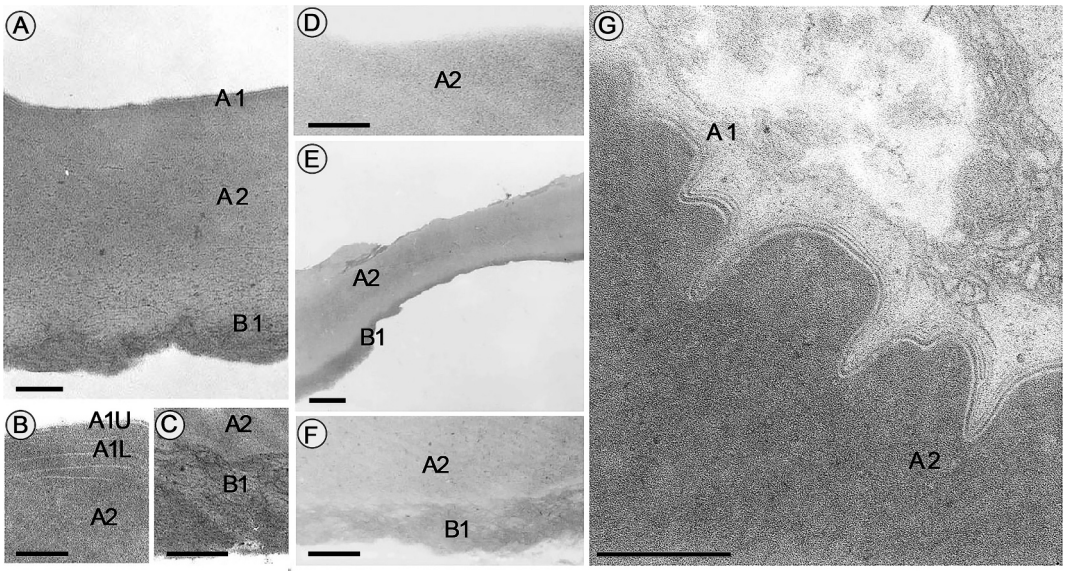

Fig. 5. Differences of cuticle ultrastructures between taxa in Ginkgoales and Coniferales (Cheirolepidiaceae) (modified after Guignard and Zhou (2005); Wang et al. (2005); Yang et al. (2009)). (A-C) *Ginkgo yimaensis* Zhou and Zhang. (D–F) *Sphenobaiera huangii* (Sze) Hsu. (G) *Pseudofrenelopsis dalatzensis* (Chow et Tsao) Cao ex Zhou. A1 is polylamellar layer, A2 is granular layer, B1 is fibrilous layer, A1U and A1L are upper and lower sublayers of A1 polylamellar layer respectively. Scale bar = 200 nm in A, B, C, G; Scale bar = 100 nm in D; Scale bar = 2 μm in E; Scale bar = 500 nm in F.

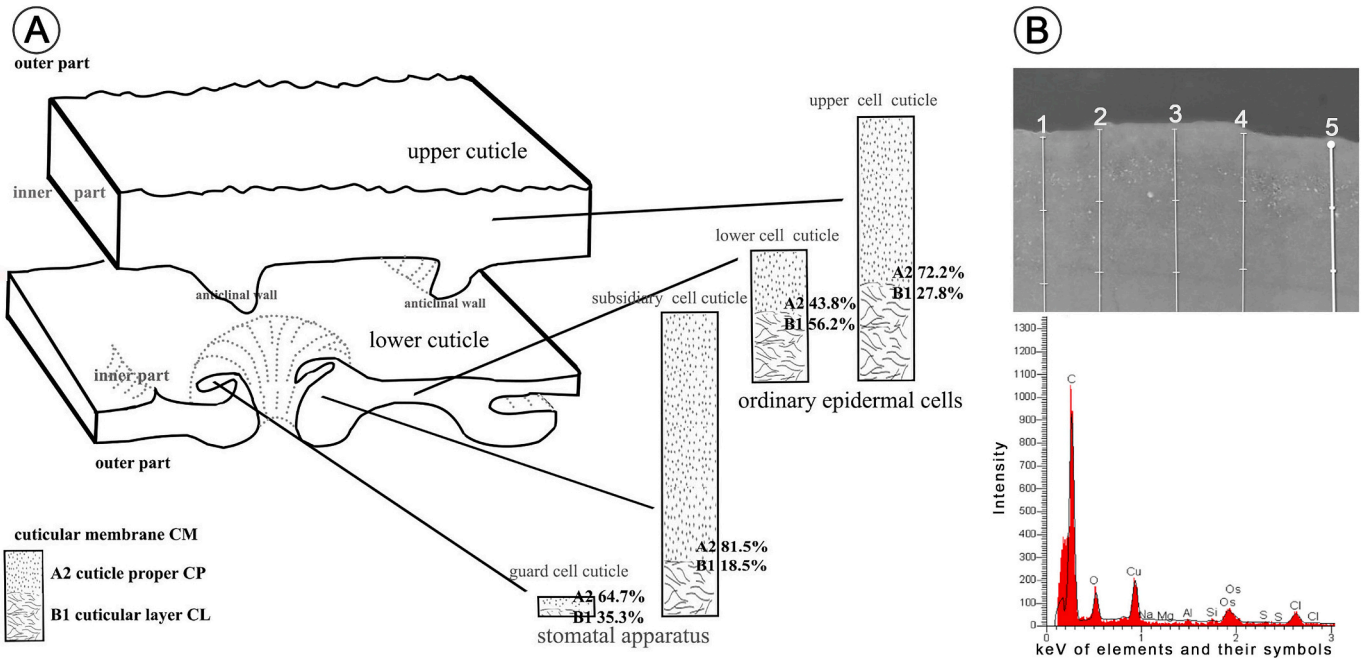

Fig. 6. (A) Three-dimensional reconstruction of cuticle ultrastructure based on fossil gingkoalean taxon *Baiera furcata* (Lindley et Hutton) Braun (after Guignard, 2019). (B) The Energy Dispersive Spectroscopy (EDS) of cuticle chemical elements based on five spectra of each cuticle layer (top right) and one example of spectrum (bottom right); from fossil *Cycadopteris obtusifolia* (Andrae) Popa from Romania; material of Mihai Popa.

uncleared cuticle (Zhang et al., 2020; Fig. 3A-C and E-G vs. Fig. 3L). As such, it is best to try multiple forms of microscopy.

4.3. Scanning electron microscopy (SEM)

4.3.1. SEM observation on clean leaves

SEM of clean leaf cuticle is particularly good for estimating stomatal size because the SEM often captures the complete stomatal anatomy well (Fig. 3M-O and Q-S). This is especially true for taxa with sunken stomata and overlapping papillae, like in Ginkgoales, which can be otherwise hard to observe under transmitted light and epifluorescence microscopy (Barclay and Wing, 2016; Matthaeus et al., 2020).

4.3.2. SEM observation on uncleared leaves

For non-fluorescing cuticles that cannot be destructively sampled, SEM is a viable choice, but will be limited to the external surface (e.g., Zhang et al., 2020; Fig. 3P).

4.4. Transmission electron microscopy (TEM)

Fossil cuticle ultrastructure has been studied with TEM since the 1980s (Archangelsky and Taylor, 1986; Archangelsky et al., 1986),

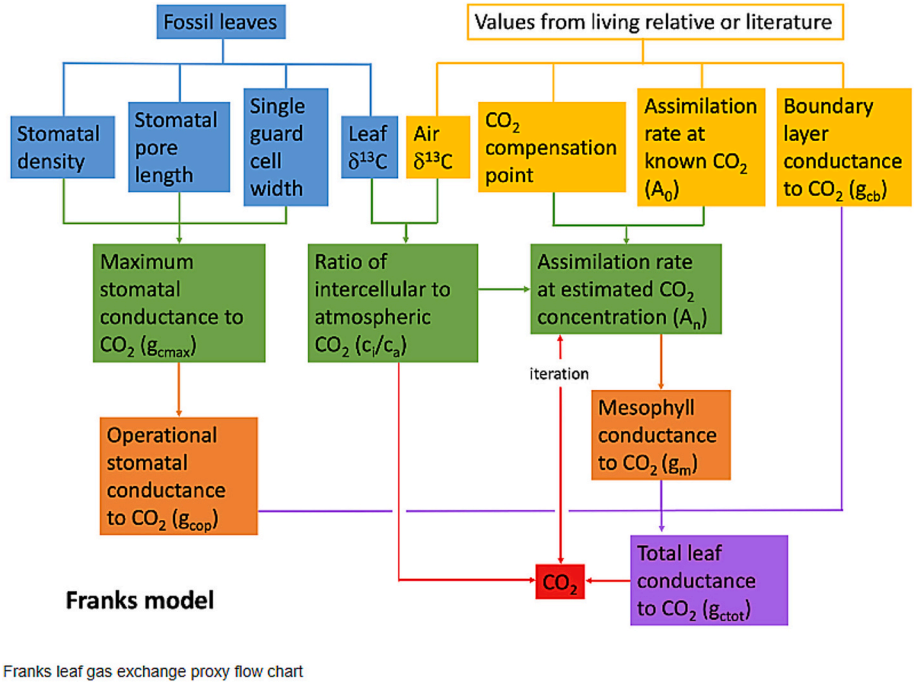

Fig. 7. Flow chart for the Franks CO_2 model (see also paleo-co2.org/proxiesLeafGas). Fossil measurements are in blue, inferred inputs in yellow. Other colors represent intermediate steps along the way to estimating CO_2 (in red). (For interpretation of the references to colour in this figure legend, the reader is referred to the web version of this article.)

primarily for taxonomic and environmental analyses. Preparation techniques for cuticle are largely adapted from classical procedures (Guignard, 2019, see his Table 1). Guignard (2021) further adapted the earlier techniques of Lugardon (1971) with images explaining the different steps. This technique creates large quantities of ultrathin cross-sections, even for plants with fragile cuticle. It is applicable to any plant cuticle (e.g., leaf, axis, flower parts, seed and fruit), fossil or living, including dried herbarium specimens.

After cleaning the cuticle (see Section 3.3), further preparation for TEM observation can be summarized as: 1) the fixation of cuticle material; 2) the embedding in resin in order to deliver precise and accurate cuticle (ultra)thin sections; 3) the sectioning by diamond knife to obtain two types of cross-sections, including: (a) thin section of 1 μm thick for glass slide observations by light microscope at low magnification to detect suitable areas for further high-magnification TEM observation, and/or (b) ultrathin sections of 60–70 nm thick for TEM observations; and 4) the staining with uranyl acetate and lead citrate to enhance the contrast with the electrons of the microscope.

Although low magnifications of cuticle usually show very uniform structure, the high magnifications obtained by TEM (can exceed 100,000×) reveal further ultrastructures composed of layers and sub-layers (Fig. 4; see also Guignard, 2019 Plate I). The terminology of ultrastructure is related to the location and morphology of the structures observed. The whole cuticle (= cuticular membrane) can be comprised of an outer cuticle proper and an inner cuticular layer. The outer cuticle proper in turn can include the polylamellar (A1) and granular (A2) layers; underneath, the cuticular layer can include the fibrilous (B1) and granular (B2) layers (Fig. 4). The order of these layers may vary across taxa. For instance, in the conifer family Cheirolepidiaceae, the cuticle ultrastructure contains A1-A2-B1-B2 layers and the outermost A1 layer is wavy (e.g., Fig. 5G). In contrast, the cuticle ultrastructure of Ginkgoales is comprised of either A2-B1 or A1U-A1L-A2-B1 (where U = upper and L = lower sublayers), depending on the genus (Wang et al., 2005; Fig. 5).

Because each section corresponds to a very small area of the cuticle (a few millimeters wide, which is the maximum size of a grid inserted in the microscope), several connected sections are needed for three-dimensional reconstruction (Fig. 6A). Ultrastructure can be compared across localities to reveal environmental differences, e.g., volcanic vs. non-volcanic, or hotter vs. cooler (Guignard et al., 2024). Additionally, the Energy Dispersive Spectroscopy (EDS) of cuticle chemical elements in each layer or sub-layer (Fig. 6B) can aid in taxonomic or environmental interpretation. In this case, no stain should be used to avoid chemical contamination.

4.5. *Fourier transform infrared (FTIR) spectroscopy*

FTIR analysis offers the opportunity to undertake chemical analysis of cuticles and leaf tissue in a cost-effective, timely, and non-destructive manner. For a broad introduction to the topic of FTIR and the wider field of vibrational spectroscopy in paleontological research, see Marshall and Marshall (2015); for a wider understanding of molecular palaeontology, see Gupta (2014). FTIR analysis can be undertaken via three routes: transmission, reflectance, and attenuated total reflectance (ATR). From the standpoint of cuticle analysis, ATR is the preferred method. Spectra are interpreted by linking wavenumber to functional groups and then these are linked to structural components of the cuticle (e.g. cutin, waxes, polysaccharides, and phenolic compounds) via consultation of the literature (Heredia-Guerrero et al., 2014; Vajda et al., 2017). For example, peaks relating to aliphatic compounds in cutin and waxes are located at 2920 cm^{-1} (CH_2 asymmetric stretching), 2850 cm^{-1} (CH_2 symmetric stretching), 1460 cm^{-1}, and 1370 cm^{-1} (both CH_2 bending).

For paleobotany, FTIR has been used to interrogate the chemical composition of cuticle to understand a variety of issues linked to taxonomy (e.g., Zodrow et al., 2010; Vajda et al., 2017; Loron et al., 2023), paleoenvironment / paleoclimate reconstruction (e.g., Jardine et al., 2019; Vajda et al., 2021), and the taphonomic and diagenetic processes responsible for converting the cuticle biopolymer into a geopolymer (e.g., Zodrow et al., 2009). Recent work has used the technique as a tool for exploring plant-animal interactions (D'Angelo et al., 2024a; Zhao et al., 2024). Additionally, important methodological advances have been

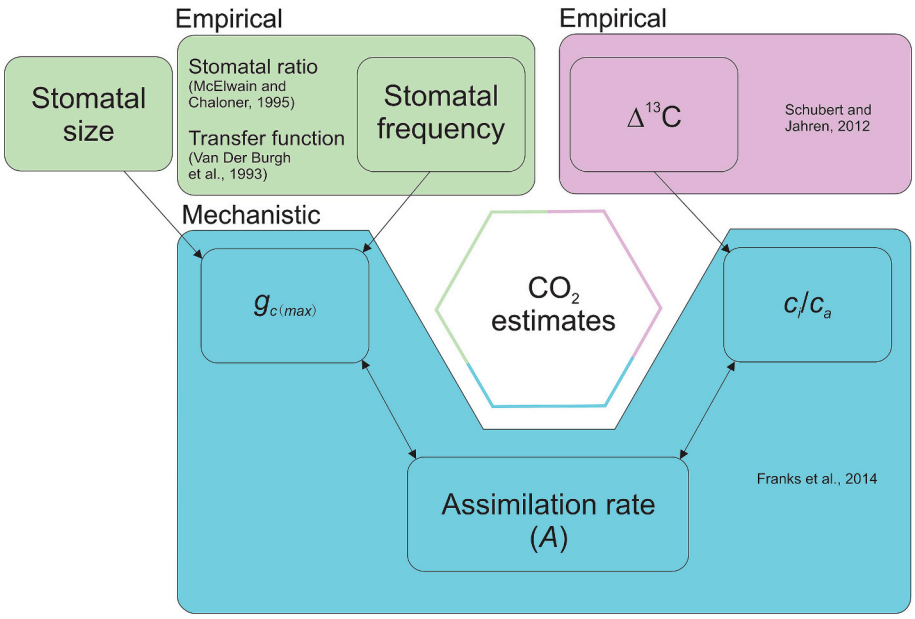

Fig. 8. Simplified flow chart for the Franks CO_2 model that focuses on the measured variables (blue boxes in Fig. 10). Modified from Porter et al. (2019). (For interpretation of the references to colour in this figure legend, the reader is referred to the web version of this article.)

made in isolating the leaf fossil or cuticle from the host rock, in order to understand how different laboratory processing techniques can affect cuticle chemistry and how these differences can be minimized for FTIR studies (Cavalcante et al., 2023).

In chemotaxonomy, recent advances in machine learning offer the opportunity to refine our understanding of taxonomy and develop tools to classify poorly resolved taxa (Katsi et al., 2024; Scoble et al., 2024). This taxonomic information may help in connecting isolated plant organs to aid whole-plant reconstructions as well as in identifying robust nearest living relatives to enable better informed choices of, for example, ecophysiology traits required for the calculation of paleoatmospheric CO_2 concentration (see Section 5). Because FTIR is non-destructive, the opportunity to combine multiple methodological approaches is an obvious advantage. For example, a single fossil leaf could be: (1) analyzed via ATR-FTIR; then (2) cleared to allow for morphological observations and measurements of the stomatal pore complex; and finally (3) destructively sampled for carbon isotope analysis.

5. The Franks leaf gas-exchange model for reconstructing CO_2

5.1. Brief description of model

An important application of fossil cuticle is the reconstruction of paleoatmospheric CO_2 concentration (see Section 1). These proxies were originally based solely on stomatal frequency (stomatal density, stomatal index, and stomatal ratio) and calibrated empirically in a nearest living relative (for a review, see McElwain and Steinthorsdottir, 2017). More recently, new CO_2 proxies have been developed based on a broader leaf gas-exchange model (Konrad et al., 2008; Franks et al., 2014; Konrad et al., 2017; Konrad et al., 2021). These proxies link the carbon assimilation rate (A, μmol m^{-2} s^{-1}) to: the total operational conductance to CO_2 diffusion from the atmosphere to the site of photosynthesis ($g_{c(tot)}$, mol m^{-2} s^{-1}), and the difference in CO_2 concentration (μmol mol^{-1}, or ppm) between the atmosphere (c_a) and intercellular spaces (c_i) (Farquhar and Sharkey, 1982):

$$A = g_{c(tot)} \times (c_a - c_i) \quad (1)$$

Solving for atmospheric CO_2 yields:

$$c_a = \frac{A}{g_{c(tot)} \times (1 - c_i/c_a)} \quad (2)$$

The Franks et al. (2014) model for CO_2 reconstruction is based directly on Eq. (2). A full model description is given in Franks et al. (2014) and in the supplements of Maxbauer et al. (2014) and Kowalczyk et al. (2018). In short, stomatal density and stomatal size (pore length and single guard cell width) of both sides of a leaf geometrically constrain maximum stomatal conductance ($g_{c(max)}$), which is then scaled to operational stomatal conductance ($g_{c(op)}$) based on measurements in living plants; this quantity is added to the mesophyll (g_m) and boundary layer (g_{cb}) conductances to yield $g_{c(tot)}$. The assimilation rate A is based on measurements in living plants at present-day CO_2 (A_0) multiplied by a CO_2 fertilization factor that is informed by a mechanistic model. Lastly, c_i/c_a is computed from measured leaf $\delta^{13}C$ and estimated paleoatmospheric $\delta^{13}C$. Fig. 7 summarizes how direct measurements on fossils are combined with inferred inputs to estimate CO_2. Users can run the model using R scripts presented in the supplement of Kowalczyk et al. (2018). Other leaf gas-exchange proxies for CO_2 (Konrad et al., 2008; Konrad et al., 2017) share a similar conceptual framework (Konrad et al., 2021) and require similar measured variables (e.g., leaf $\delta^{13}C$ and stomatal size and density); as such, the recommendations made here for the Franks model generally apply to these models too.

5.2. Strengths of the Franks model

Eq. 2 dictates that stomatal density is related to CO_2 following an inverse power law (Royer et al., 2019; Konrad et al., 2021), consistent with many empirical calibrations (e.g., Barclay and Wing, 2016). A typical error rate (accuracy) when the Franks model is applied to living plants with a known growth CO_2 concentration is ~20 % (Royer et al., 2019), with a precision at 95 % confidence of about +35 / -25 % of the median estimate (Franks et al., 2014). A similar accuracy is observed when comparing estimates of CO_2 to ice-core measurements during the Pleistocene-Holocene transition (Franks et al., 2014). Because the Franks model is mostly mechanistic in nature, it can be applied to most C_3 leaf fossils and the size of its uncertainties in living plants probably scales to that in fossil plants. In contrast, uncertainties associated with the empirically calibrated CO_2 proxies (e.g., stomatal index and stomatal ratio) are more likely to be falsely optimistic because they assume no

change in the calibrated (empirical) response over geologic time. The Franks model is also based on multiple measured variables, in contrast to the mostly univariate empirical proxies (Fig. 8). In principle, this means that the Franks model should be better equipped at capturing the complex interplay in the morphological and physiological responses to CO_2 change. For example, even if the stomatal density or carbon isotope fractionation in an extant species does not respond to CO_2, the species may still predict CO_2 accurately when placed within the framework of the Franks model (e.g., Milligan et al., 2019). Estimates of CO_2 based on stomatal frequency alone are often low during periods known for global warmth like the Paleocene (e.g., Royer et al., 2001), while estimates from gas-exchange proxies are not (Kowalczyk et al., 2018; Milligan et al., 2019; Konrad et al., 2021).

5.3. Value choices for inferred inputs

The Franks model is not entirely mechanistic. Nearest living relatives inform value choices for A_0, $g_{c(op)}/g_{c(max)}$ (also called ζ or s4), g_m, and the scalar between pore length and maximum pore area. Sensitivity analyses point to the first two as the most critical: their uncertainties can propagate to large differences in estimated CO_2 (e.g., Maxbauer et al., 2014; McElwain et al., 2016; Kowalczyk et al., 2018; Milligan et al., 2019). For fossil taxa with close nearest living relatives, prescribing values based on measurements from their living relatives is optimal. For A_0, species within the same genus provide relatively lower risk of systematic error (<20 % potential skew), whereas within the same family or order can produce offsets that are skewed by >50 % (Reichgelt and D'Andrea, 2019); constraints on the paleoecology, such as plant habit and the type of ecosystem, can greatly reduce the risk of systematic skew (<10 %; Reichgelt and D'Andrea, 2019).

A_0 and ζ measurements on living plants for model constraints should be made on sun-exposed leaves because the scaling between assimilation rate and CO_2 in the Franks model assumes leaves that are not light limited (Eq. 6 in Franks et al., 2014). This also means that the fossils should be sun-adapted. Fortunately, the majority of leaves in the fossil record are sun-adapted (Kürschner, 1997) because—relative to shade leaves—they are more numerous, more resistant to decay, and more likely to be carried by wind to a depositional setting (Ferguson, 1985; Greenwood, 1992). Shade morphotypes can sometimes be differentiated from sun leaves of the same species at the same site based on their large, undulated epidermal cells, low leaf $\delta^{13}C$, and low vein, trichome, and stomatal density (Kürschner, 1997; Nguyen Tu et al., 2004; Sack et al., 2006; Graham et al., 2014; Milligan et al., 2021; compare Fig. 3F to 3G, a sun and shade morphotype respectively of *Quercus pseudocastanea* from Kürschner, 1997). In addition, mesophyll structure such as multi-layered vs. single layered palisade parenchyma can help to identify the leaf morphotype (Kürschner, 1997). If there is a bimodal distribution in these traits across leaves in a single taxon at a single site, the putative shade leaves should be excluded. We recommend particular care for fossil assemblages from dense, multi-stratal forests because shade leaves typically assimilate carbon slower and are likely to assimilate soil- or plant-respired CO_2 from their CO_2-enriched forest understory, ultimately resulting in anomalously low leaf $\delta^{13}C$ (Graham et al., 2014; Royer et al., 2019). The resulting CO_2 reconstruction from shade leaves will therefore be falsely high relative to the well-mixed atmosphere (e.g., Royer et al., 2019; Reichgelt et al., 2020).

If prescription of inferred inputs from a close nearest living relative is not possible, we recommend using values from ecological equivalents or from broader taxonomic groups (e.g., Franks et al., 2014; Murray et al., 2019; Reichgelt and D'Andrea, 2019; Murray et al., 2020). For example, Reichgelt and D'Andrea (2019) report an A_0 dataset for ~2500 extant species across a broad taxonomic spectrum together with broad ecological classifications. Alternatively, A can be estimated for fossils of unknown affinities using scaling relationships for extant taxa between morphological traits that influence the movement of water and/or CO_2 in the leaf, such as vein density and vein-to-stomatal distance (Brodribb and Feild, 2010; McElwain et al., 2015; McElwain et al., 2016; Montañez et al., 2016; Wilson et al., 2017).

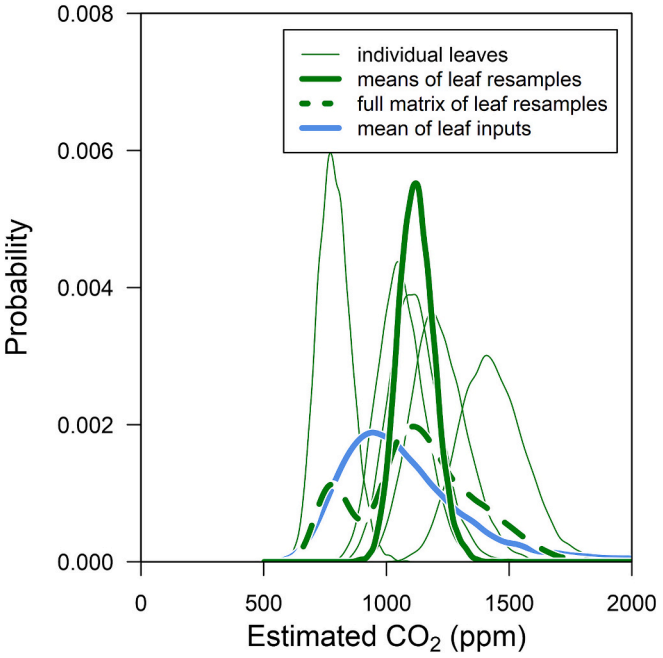

Fig. 9. Different ways of estimating CO_2 with multiple leaves of a single species. The example here is five extant *Cedrus deodara* (Roxburgh) G.Don leaves grown at 1000 ppm CO_2 (Milligan et al., 2019). Probability density functions (PDFs) of estimated CO_2 from individual leaves (thin green lines; uncertainties in the morphological and physiological inputs are assumed to be 5 % of their mean values) are compared to three ways of creating a species-level pdf (thick lines). Blue: leaf-level inputs (stomatal density, stomatal size, etc.) are averaged first and then the Franks model is run once. Dashed green: The resamples used to create the leaf-level PDFs are combined into a single matrix (5 × 10,000 in this case) and a PDF is created directly from this larger matrix. Solid green: Means of each of the 10,000 resamples from the larger matrix are calculated first (where–in this case–each mean is based on five CO_2 resamples) and then a PDF is created from the string of 10,000 means. (For interpretation of the references to colour in this figure legend, the reader is referred to the web version of this article.)

Presently, the Franks model assumes a single value with no uncertainty for the carbon isotopic discrimination against ^{13}C by the enzyme RuBisCo (30 ‰). Within major taxonomic groups such as gymnosperms, overall isotopic discrimination can vary by over 10 ‰ in plants grown under natural "common garden experiment" conditions (Sheldon et al., 2020). Part of this range is likely due to differences in the fractionation of RuBisCo, which has only been directly observed for a relatively small number of species. Varying this fractionation from 27 to 30 ‰ (e.g., Roeske and O'leary, 1984; discussed at length in Farquhar et al., 1989; Guy et al., 1987) can lead to variations in estimated CO_2 exceeding 25 % (Porter et al., 2019; Stein et al., 2024; Machesky et al., 2025). Thus, care should be taken in assigning a value and uncertainty for this fractionation, especially for fossils that lack modern relatives.

5.4. Constraining uncertainty in measured inputs

Among the measured variables in the Franks model, CO_2 estimates are often most sensitive to stomatal density (Maxbauer et al., 2014; Kowalczyk et al., 2018; Milligan et al., 2019; Zhang et al., 2024) and phylogenetic differences in carbon isotope discrimination (Porter et al., 2019). Variance in stomatal density contributes more than any other measured input to the overall uncertainty in reconstructed CO_2 than any other measured input. Thus, it is important to take appropriate steps to reduce bias and noise in stomatal density measurements, for example by

preparing leaves for high-quality images (Section 3) and analyzing enough leaves and fields-of-view (Section 6.1–6.2).

Machesky et al. (in press) measured stomatal traits in three species with contrasting leaf morphology (*Ginkgo biloba* Linnaeus, *Quercus alba* Linnaeus, and *Zingiber mioga* (Thunberg) Roscoe) and found some traits to be more variable within species (pore length and guard cell pair width) than others (guard cell length and stomatal density). Also, any external surface observation on untreated leaves, including SEM (Section 4.4.1), epifluorescence (Section 4.2.1), and dental putty impressions (Section 4.3), can yield inaccurate measurements of guard cell width and length, especially for taxa with sunken stomata like in Ginkgoales (ginkgos), Coniferales (conifers), Pteridospermales (seed ferns), and Bennettitales (Stein et al., 2024; Machesky et al., 2025). Thus, we advise that applications of leaf gas exchange models use cleared leaves when possible.

5.5. Estimate CO_2 from leaves first, then scale to the species

Each leaf is a unique biosensor and is the fundamental unit of replication for paleo-CO_2 methods, including the Franks model. In addition, most inputs in the Franks model relate nonlinearly to CO_2 and many combinations of inputs are internally consistent with a single CO_2 concentration. For these reasons, it is best to estimate CO_2 from each leaf individually (e.g., see thin green lines in Fig. 9) and then combine leaf-level CO_2 estimates into a single species-level estimate (thick green lines in Fig. 9). This contrasts with calculating means and standard errors in the measured inputs across all leaves first and then estimating CO_2 once at the species level (thick blue line in Fig. 9). Some studies go a step further in their recommendations and suggest that the most accurate paleo-CO_2 estimates using the Franks model are those that use a fossil assemblage approach based on values from multiple species (Reichgelt et al., 2020) and multiple evolutionary groups (Porter et al., 2019) (See also section 6.3).

Here we highlight two ways to combine leaf-level probability density functions (PDFs) into a species-level PDF (see also Supplementary material 2 for input file and R code); these strategies can also be used to combine species-level PDFs, such as those from different evolutionary groups, into a site-level PDF. The first is to combine the CO_2 resamples (typically 10,000 with the Franks model) from the individual leaves into a single matrix and create a PDF directly from this matrix (thick dashed green line in Fig. 9, based here on a 5 × 10,000 matrix). This approach is conservative: consider, for example, a set of leaves with identical PDFs. This first approach will create a species-level PDF that is identical to the leaf-level PDFs; it is not sensitive to sampling effort (number of leaves). A second approach that addresses this shortcoming is to calculate the mean of each of the 10,000 resamples first and then create a PDF from the 10,000 means (thick solid green line in Fig. 9). With this "means" approach, the width of the PDF tightens as more leaves are added, much like a standard error of the mean.

6. What is the best sampling strategy for optimizing reliability against effort, both within and across leaves?

6.1. Sampling strategy within leaves

6.1.1. Morphological measurements: Location of fields-of-view

Cell size varies across most leaves in a coherent manner. Generally, epidermal cell size is smallest near the leaf margins, especially towards the tip (e.g., Salisbury, 1928; Tichá, 1982; Weyers and Meidner, 1990; Poole et al., 1996; Weyers and Lawson, 1997; Royer et al., 2001). Therefore, cell densities (epidermal, stomatal), especially in angiosperms, are typically highest near the leaf margins. In most gymnosperm needle leaves, the mid-lamina has the least cell area variability (e.g., Salisbury, 1928; Poole et al., 1996).

In most cases, the signal-to-noise ratio is maximized by measuring cell areas and densities in the mid-lamina (Poole and Kürschner, 1999).

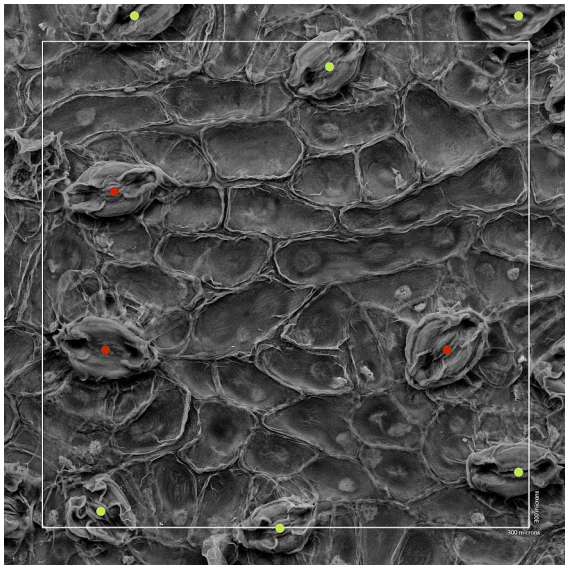

Fig. 10. Different ways for calculating stomatal density (*Ginkgo biloba* RSB 1343 leaf A spot 7 under SEM from Barclay and Wing, 2016). The white box is the field-of-view (0.3 × 0.3 mm). Stomatal complexes marked with red dots are fully within the field-of-view ($n = 3$); stomata with yellow dots are only partly within the field-of-view ($n = 9$). How boundary crossers are treated can scale to large differences in estimated stomatal density at the leaf and species level. (For interpretation of the references to colour in this figure legend, the reader is referred to the web version of this article.)

If one is using a calibrated response in extant leaves to extract environmental information from fossils, it is best to sample fossils in the same manner as the calibration. If one wishes to know average whole-leaf values, measuring only mid-lamina can return slightly biased results (e.g., <5 % in Poole et al., 2000).

6.1.2. Strategies for measuring stomatal density

When measuring stomatal density, typically the regions overlying major veins and near leaf margins—which often lack stomata and whose epidermal cells have distinctive shapes—are avoided. When stomata are present in these regions, they often carry out functions not directly related to gas exchange, most notably guttation (Feild et al., 2005; Reichgelt et al., 2023). Calibrations in extant vegetation between stomatal frequency and CO_2 are usually based on intercostal regions, so it is in the best interest for fossil paleo-CO_2 applications of these calibrations to follow suit.

This is not a universal rule, though, and there may be times when including the costal regions makes sense. In the Franks CO_2 model, stomatal size and density is used to estimate the maximum stomatal conductance to CO_2 ($g_{c(max)}$), which is then scaled to operational stomatal conductance ($g_{c(op)}$) based on gas-exchange measurements in living plants ($g_{c(op)}/g_{c(max)}$ or ζ or s4) (Murray et al., 2020, see Section 5.1). These $g_{c(op)}$ measurements are typically made by placing a whole leaf (or a large piece of a leaf) inside the chamber of an infrared gas analyzer or porometer; importantly, major veins are typically included. For fossil studies applying the Franks CO_2 model, avoiding major veins when measuring stomatal density—following convention—is generally fine so long as the fraction of vein tissue without stomata has not changed significantly between the fossil and extant taxon used to inform $g_{c(op)}/g_{c(max)}$. If it has changed, then the $g_{c(op)}/g_{c(max)}$ scalar may be inappropriate for the fossil. Leaves with stomatal bands, for example many conifers, are the most likely to violate this assumed constancy in vein tissue fraction. In these cases, a representation of whole-leaf stomatal density needs to be estimated (Kouwenberg et al., 2003; Maxbauer et al., 2014; Liang et al., 2022a).

When measuring stomatal or epidermal cell density, a standardized

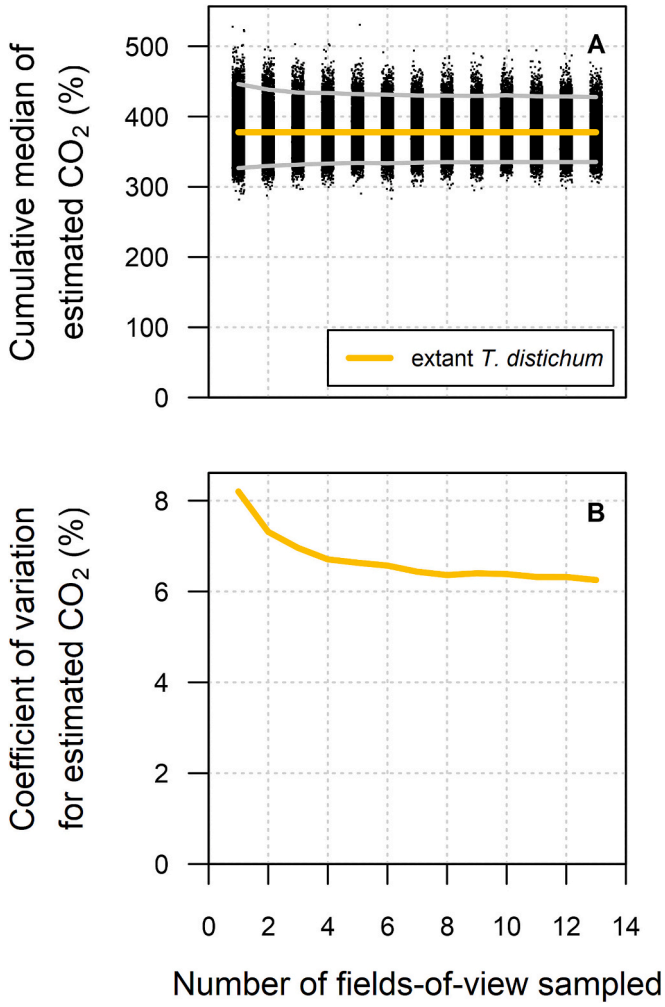

Fig. 11. Sensitivity of estimated CO_2 in the Franks model to the number of measurements of stomatal density for a single extant leaf of *Taxodium distichum* (from Liang et al., 2022a). Each measurement of stomatal density is based on one field-of-view. (A) The gold horizontal line is the median estimated CO_2 based on the full data set (all fields-of-view). The black vertical clouds contain individual estimates of CO_2 based on random field-of-view draws at each level of subsampling (jittered); the gray envelopes contain 95 % of the individual CO_2 estimates. (B) Data in panel A expressed as a coefficient of variation (standard deviation divided by the mean). (For interpretation of the references to colour in this figure legend, the reader is referred to the web version of this article.)

approach is needed to account for cells overlapping the field-of-view border. Kubínová (1994) and Poole and Kürschner (1999) recommend counting all partials along two edges (one long edge and one short edge, if rectangular) but none along the other two edges (i.e., "edges" approach). A similar strategy is to only count partials that are more than 50 % inside the field-of-view (i.e., "halves" approach). Other strategies include "all in" and "all out": including all or no partials, respectively. We tested these four counting strategies on five extant *Ginkgo biloba* leaves reported in Barclay and Wing (2016) (sample RSB 1343; each leaf contains seven intercostal fields-of-view). We measured higher stomatal densities for the "all in" versus "all out" approach (mean = 95 and 57 mm^{-2}, respectively). Fig. 10 shows an extreme example of the differences, where stomata completely within the field-of-view are marked with red dots and partial stomata with yellow dots. We measured intermediate densities for the "two edges" and "halves" approaches (mean = 73 and 75 mm^{-2}, respectively). The differences across these four counting techniques propagate to large differences in estimated CO_2 when using the Franks model, with the sample medians ranging from

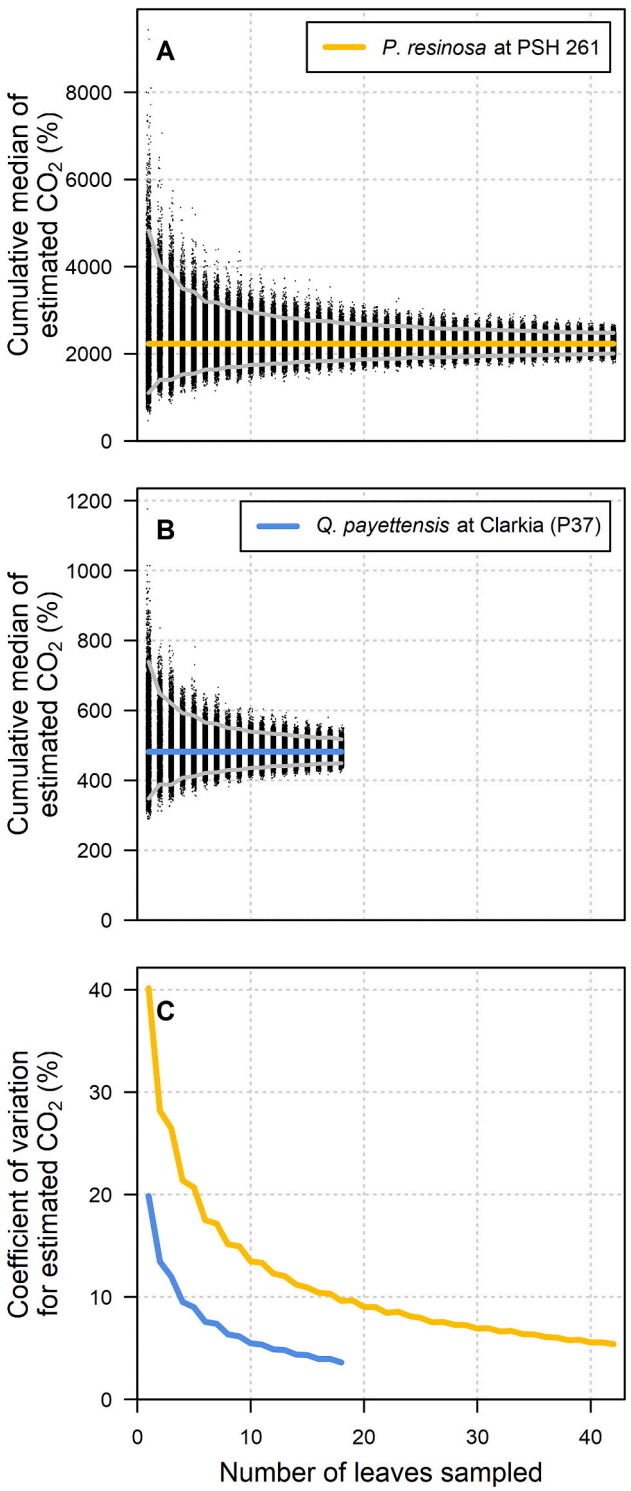

Fig. 12. Sensitivity of estimated CO_2 in the Franks model to the number of leaves analyzed. (A) 42 *Pseudotorellia* leaves from the mid-Cretaceous PSH 261 site in Mongolia (Zhang et al., 2024). (B) 18 *Quercus payettensis* leaves from the mid-Miocene P37 site at Clarkia, Idaho (Steinthorsdottir et al., 2021). The gold and blue horizontal lines are the median estimated CO_2 based on the full data sets (all 42 leaves). The black vertical clouds contain individual estimates of CO_2 based on random draws of leaves at each level of subsampling (jittered); the gray envelopes contain 95 % of the individual CO_2 estimates. (C) Data in panels A and B expressed as a coefficient of variation (standard deviation divided by the mean). (For interpretation of the references to colour in this figure legend, the reader is referred to the web version of this article.)

467 to 693 ppm. In principle, the "two edges" and "halves" approaches should best represent the true whole-leaf stomatal density; for example, if a grid of fields-of-view is laid out across an entire leaf, these two approaches will most accurately represent the stomata split across fields-of-view.

A large field-of-view is preferable (at least 0.03 mm^2; Poole and Kürschner, 1999) because this minimizes the influences of edges (see previous paragraph) and the intraleaf spatial patterns in cell morphology (see Section 6.1.1). If coastal or damaged regions cannot be avoided in a field-of-view, their associated areas need to be digitally removed before measuring the densities of cells, stomata, etc.

Multiple fields-of-view per leaf or leaf fragment should be measured. We recommend the cumulative mean to guide this decision (e.g., Poole and Kürschner, 1999; Bonis et al., 2010). In other words, in the case of using stomatal frequency to reconstruct atmospheric CO_2, a running mean of CO_2 inferences should be plotted against sampling effort (number of fields-of-view) and individual fields-of-view should be added until the mean stabilizes. Fig. 11 highlights one example with the Franks model for a single extant *Taxodium distichum* (Linnaeus) Richard leaf reported by Liang et al. (2022a) (leaf L2 BM; see Supplementary material 3 for input file and R code). These authors measured stomatal density from thirteen fields-of-view distributed across the leaf. Here, after four or five fields-of-view, further gains in precision diminish rapidly as gauged by the coefficient of variation (Fig. 11B). One key strength of a sensitivity analysis like this is that it can be carried out as fields-of-view are added, allowing a researcher in real time to optimize precision against effort.

6.1.3. Leaf $\delta^{13}C$ measurements

When preparing fossil leaves for carbon isotopic analysis, chemical treatments should be avoided whenever possible because the resultant reactions can affect tissue $\delta^{13}C$ (Barral et al., 2015); this is also true with nitrogen and $\delta^{15}N$ (Brodie et al., 2011a; Brodie et al., 2011b; Schlacher and Connolly, 2014; Vaiglova et al., 2014; Fujisaki et al., 2022). These chemical effects are particularly strong with Schulze's solution (HNO_3 + $KClO_3$; Barral et al., 2015). Fortunately, hydrochloric acid (HCl)–which is critical for removing carbonates before carbon isotopic analysis–has little-to-no effect on organic $\delta^{13}C$ (Barral et al., 2015; Montañez et al., 2016). Hydrogen fluoride (HF) has some effect, slightly increasing the intra- and inter-leaf variances (Barral et al., 2015). If both morphology and $\delta^{13}C$ are measured on the same leaves, the tissue for $\delta^{13}C$ should be subsampled before any treatments are applied to clear the mesophyll whenever possible (unless the goal is to measure cuticle $\delta^{13}C$).

Major veins and petioles have a higher $\delta^{13}C$ (by up to ~3 ‰) than the rest of the leaf (Gröcke, 2020; Royer and Hren, 2022). To maximize the signal-to-noise ratio, petioles and major veins should be avoided unless the entire leaf can be measured; in most leaves tested, the remaining intercostal tissue varies by ~1 ‰ (Barral et al., 2015; Royer and Hren, 2022). Avoiding large veins and the petiole will bias the $\delta^{13}C$ measurements towards lower values relative to the whole leaf, but only by a small amount (~0.6 ‰; Royer and Hren, 2022). More than one sample per fossil leaf should be measured for $\delta^{13}C$, if possible. If the preserved leaf mass is small, analysis by nano-combustion gas chromatography and isotope ratio mass spectrometry may allow for multiple measurements as this approach permits nanogram analysis of particulate organic matter (e.g., van Roij et al., 2017).

Leaf cuticle contains cutin, cuticular waxes, and polysaccharides (Esau, 1977; Kolattukudy and Espelie, 1989; Jeffree, 1996; Kolattukudy et al., 1997; Rozema et al., 1997), which all differ in their $\delta^{13}C$ (DeNiro and Epstein, 1977; Dawson et al., 2002). Compound-specific isotope analyses are widespread in paleoclimate studies (e.g., Tareq et al., 2011; Gori et al., 2013; Diefendorf and Freimuth, 2017) because they account for these differences, which can otherwise introduce uncertainty when measuring bulk $\delta^{13}C$ from fossils comprised of partly degraded carbon, including cuticle. However, measurements from living plant leaves

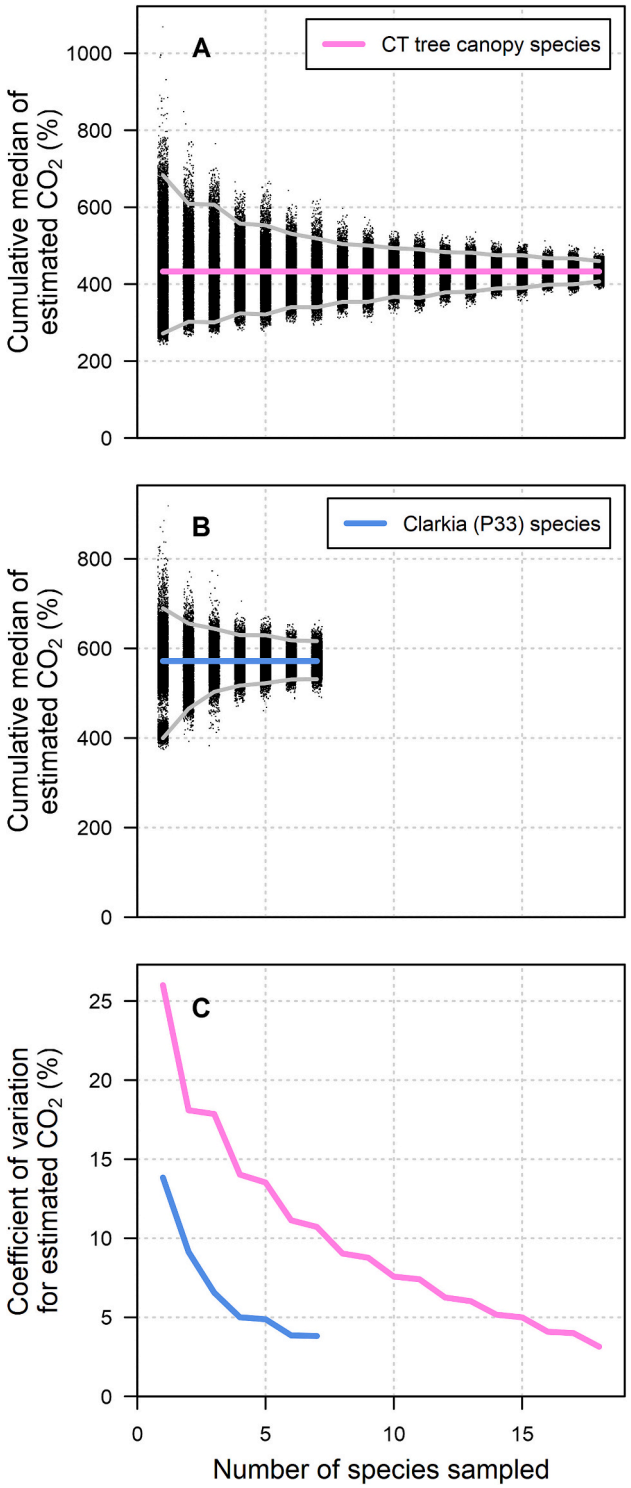

Fig. 13. Sensitivity of estimated CO_2 in the Franks model to the number of species analyzed. (A) 18 extant tree canopy species from Connecticut (Royer et al., 2019). (B) Seven species from the mid-Miocene P33 site at Clarkia, Idaho (Steinthorsdottir et al., 2021; Liang et al., 2022a). The pink and blue horizontal lines are the median estimated CO_2 based on the full data sets (all species). The black vertical clouds contain individual estimates of CO_2 based on random draws of species at each level of subsampling (jittered); the gray envelopes contain 95 % of the individual CO_2 estimates. (C) Data in panels A and B expressed as a coefficient of variation (standard deviation divided by the mean). (For interpretation of the references to colour in this figure legend, the reader is referred to the web version of this article.)

suggest that the isotopic offset between whole leaves and cuticles is typically <1 ‰ (Royer and Hren, 2017). Furthermore, in a study mimicking degradation of Lagerstätten fossils, $\delta^{13}C$ remained virtually unchanged even as polysaccharides preferentially decayed during early diagenesis (Witkowski et al., 2022).

Bulk $\delta^{13}C$ values are useful because they are the most commonly reported metric of $\delta^{13}C$, and therefore serve as a common reference frame; they are also less affected by differential compound presence or measurement tools (Bowling et al., 2008). On the other hand, compound-specific analyses are very useful when looking at the ecosystem scale or within soils as sediments (rather than whole fossils), as these values can give insight into the composition of ecosystems and any relative shifts, and are unencumbered by entangled temporal and spatial uncertainties that are more impactful on bulk $\delta^{13}C$ (e.g., Diefendorf and Freimuth, 2017; Whiteman et al., 2019).

6.2. How many leaves are needed for a species-level inference? Example using the Franks model

A minimum of five leaves or leaflets per species is generally suggested for reliable species-level paleo-CO_2 estimates (Beerling and Royer, 2002; Slodownik et al., 2020). Similar to determining the number of fields-of-view (Section 6.1.2), we recommend the cumulative mean to guide this decision. Fig. 12 showcases two examples with the Franks CO_2 model (see Supplementary material 4 for input file and R code). Zhang et al. (2024) estimated CO_2 for a mid-Cretaceous site (PSH 261) in Mongolia using 42 *Pseudotorellia resinosa* leaves (Fig. 12A). Here, the black clouds and gray uncertainty envelope don't flatten appreciably until about 10–15 leaves, well above the recommended value of five. This is due to the fossils' very low stomatal density (mean = 13.4 mm^{-2}), causing small variations in stomatal density across leaves to propagate to large differences in estimated CO_2 levels.

We contrast these results to those from Steinthorsdottir et al. (2021), who reconstructed CO_2 for the mid-Miocene Clarkia site (P37) in Idaho using 18 leaves of *Quercus payettensis* Knowlton (Fig. 12B). Here, five leaves are a good minimum sampling target.

Fig. 12C is a summary of the two sites where the coefficient of variation (standard deviation divided by the mean) is used to standardize the y-axis across studies. For new studies, this kind of sensitivity analysis can be done cumulatively, as leaves are added. A key message is that five leaves is a good minimum target, but more than five may be necessary if the uncertainty remains high.

In the absence of leaf macrofossils, fragmentary mesofossils can provide important constraints on environmental conditions such as CO_2 concentration (e.g., McElwain et al., 2005; Barclay et al., 2010; Richey et al., 2018). With fragments, their relative position on the original leaf (base, tip, middle, etc.) can be difficult to reconstruct, and it is usually impossible to know if multiple fragments come from one or many leaves. Also, because fragments are small, the potential number of fields-of-view is typically low. Together, this means that it is difficult to test the sensitivity to number of leaves and fields-of-view; only the test for number of fragments is robust.

6.3. How many species are needed for a site-level inference? Example using the Franks model

The number of species needed to generate reliable site-level inferences such as estimated CO_2 concentration depends on multiple factors, including sampling effort at the leaf level (see Section 6.2) and the sensitivity of estimated CO_2 to the model inputs (e.g., assimilation rate; see Section 5.3; see also Reichgelt and D'Andrea, 2019). Similar to the analysis for the number of leaves (Section 6.2), Fig. 13 shows a bootstrap analysis using the Franks model to estimate CO_2 for two studies that incorporated multiple species: 18 extant tree canopy species from Connecticut (Royer et al., 2019) and seven fossil species measured at Clarkia site P33 (Steinthorsdottir et al., 2021); see Supplementary material 5 for input file and R code.

It is clear that fewer species are needed at Clarkia than Connecticut. This is probably because the sampling effort at Connecticut was less (mostly 1–3 leaves per species vs. 4–16 at Clarkia). To achieve a coefficient of variation of 5 %, four species are needed at Clarkia versus 14 for extant Connecticut (Fig. 13C). If one is in the luxurious position of having multiple cuticle-bearing taxa at a single site, this kind of sensitivity analysis can be done as species are added to the database.

7. Conclusion

There are many published methods related to the study of fossil leaf cuticle, ranging from finding suitable fossils in the field to preparing fossil cuticle for microscopy and interpreting quantitative data from its chemistry and morphology. These methods naturally emerge from individual studies, typically for a single taxon or study area, and usually after much trial-and-error. Our hope is that the compiled information presented here can improve the time efficiency of the user, particularly those with less experience. With this in mind, the obvious caveat is that "mileage may vary". For example, we cannot guarantee the outcomes implied in the cuticle preparation flowcharts (Figs. 1–2) and recipes (Supplementary Table 2 in Supplementary material 1). Some ongoing trial-and-error should be expected.

Declaration of competing interest

The authors declare that they have no known competing financial interests or personal relationships that could have appeared to influence the work reported in this paper.

Acknowledgments

This project was conceived at workshops associated with the CO_2 Proxy Integration Project (CO_2PIP). Funding comes from National Science Foundation of USA (grant number FRES 2121540 to DLR and grant number FRES 2121594 to IPM), the National Natural Science Foundation of China (grant number NSFC 42202024 to XZ), and Natural Science Foundation of Jiangsu Province, China (grant number BK20221160 to XZ).

Appendix A. Supplementary data

Supplementary data to this article can be found online at https://doi.org/10.1016/j.earscirev.2025.105104.

Data availability

I have shared my code and data at the Attach File step

References

Andrews, P., 1990. Owls, Caves and Fossils. University of Chicago Press, Chicago, 231 pp.

Archangelsky, S., Taylor, T.N., 1986. Ultrastructural studies of fossil plant cuticles. II. Tarphyderma Gen. N., a Cretaceous conifer from Argentina. Am. J. Bot. 73 (11), 1577–1587.

Archangelsky, S., Taylor, T.N., Kurmann, M.H., 1986. Ultrastructural studies of fossil plant cuticles: *Ticoa Harrisii* from the early Cretaceous of Argentina. Bot. J. Linn. Soc. 92 (2), 101–116.

Archangelsky, A., Andreis, R.R., Archangelsky, S., Artabe, A., 1995. Cuticular characters adapted to volcanic stress in a new Cretaceous cycad leaf from Patagonia, Argentina. Considerations on the stratigraphy and depositional history of the Baqueró Formation. Rev. Palaeobot. Palynol. 89 (3–4), 213–233.

Arens, N.C., Jahren, A.H., 2000. Carbon isotope excursion in atmospheric CO_2 at the Cretaceous-Tertiary boundary: evidence from terrestrial sediments. Palaios 15 (4), 314–322.

Arens, N.C., Jahren, A.H., Amundson, R., 2000. Can C_3 plants faithfully record the carbon isotopic composition of atmospheric carbon dioxide? Paleobiology 26 (1), 137–164.

Barale, G., Baldoni, A., 1993. Ultrastructure of some bennettitalean cuticle from the lower cretaceous of Argentina. Comptes Rendus de l'Académie des Sciences. Série 2, 316(8), 1171–1177.
Barclay, R.S., 2011. Testing the Driving Mechanisms for Ocean Anoxic Event 2 (94Ma) Using pCO_2 Estimates and Carbon Isotopes Derived from Fossil Plant Material in the Dakota Formation of Southwestern Utah. Ph.D. Thesis,. Northwestern University.
Barclay, R.S., Wing, S.L., 2016. Improving the *Ginkgo* CO_2 barometer: Implications for the early Cenozoic atmosphere. Earth Planet. Sci. Lett. 439, 158–171.
Barclay, R., McElwain, J., Dilcher, D., Sageman, B., 2007. The Cuticle Database: Developing an interactive tool for taxonomic and paleoenvironmental study of the fossil cuticle record. In: Jarzen, D., Manchester, S., Jarzen, S., Retallack, G. (Eds.), Advances in Paleobotany Conference 2006. CFS Courier Forschungsinstitut Senckenberg, Florida Museum Nat Hist, Gainesville, FL, pp. 39–55.
Barclay, R.S., McElwain, J.C., Sageman, B.B., 2010. Carbon sequestration activated by a volcanic CO_2 pulse during Ocean Anoxic Event 2. Nat. Geosci. 3 (3), 205–208.
Barral, A., Lécuyer, C., Gomez, B., Fourel, F., Daviero-Gomez, V., 2015. Effects of chemical preparation protocols on $\delta^{13}C$ values of plant fossil samples. Palaeogeogr. Palaeoclimatol. Palaeoecol. 438, 267–276.
Barthel, M., 1962. Epidermisuntersuchungen an einigen inkohlten Pteridospermenblättern des Oberkarbons und Perms. Geologie 11 (Beiheft 33), 1–140.
Beaulieu, J.M., Leitch, I.J., Patel, S., Pendharkar, A., Knight, C.A., 2008. Genome size is a strong predictor of cell size and stomatal density in angiosperms. New Phytol. 179 (4), 975–986.
Beerling, D.J., Royer, D.L., 2002. Reading a CO_2 signal from fossil stomata. New Phytol. 153 (3), 387–397.
Behrensmeyer, A.K., Hook, R.W., 1992. Paleoenvironmental Contexts and Taphonomic Modes. In: Behrensmeyer, A.K., Damuth, J.D., DiMichele, W.A., Potts, R., Sues, H.-D., Wing, S.L. (Eds.), Terrestrial Ecosystems through Time: Evolutionary Paleoecology of Terrestrial Plants and Animals. University of Chicago Press, Chicago, pp. 15–93.
Bernado, W.D., Rakocevic, M., Santos, A.R., Ruas, K.F., Baroni, D.F., Abraham, A.C., Pireda, S., Oliveira, D.D., Da Cunha, M., Ramalho, J.C., Campostrini, E., Rodrigues, W.P., 2021. Biomass and leaf acclimations to ultraviolet solar radiation in juvenile plants of *Coffea arabica* and *C.* canephora. Plants 10 (4), 640.
Bhadra, S., Leitch, I.J., Onstein, R.E., 2023. From genome size to trait evolution during angiosperm radiation. Trends Genet. 39 (10), 728–735.
Bonis, N.R., Van Konijnenburg-Van Cittert, J.H.A., Kurschner, W.M., 2010. Changing CO_2 conditions during the end-Triassic inferred from stomatal frequency analysis on *Lepidopteris ottonis* (Goeppert) Schimper and *Ginkgoites taeniatus* (Braun) Harris. Palaeogeogr. Palaeoclimatol. Palaeoecol. 295 (1–2), 146–161.
Bowling, D.R., Pataki, D.E., Randerson, J.T., 2008. Carbon isotopes in terrestrial ecosystem pools and CO_2 fluxes. New Phytol. 178 (1), 24–40.
Brodie, P.B., 1842. Notice of the occurrence of fossil plants in the plastic clay at Bournemouth, Hants. J. Franklin Institute 34 (3), 178–179.
Brodie, C.R., Casford, J.S.L., Lloyd, J.M., Leng, M.J., Heaton, T.H.E., Kendrick, C.P., Zong, Y.Q., 2011a. Evidence for bias in C/N, $\delta^{13}C$ and $\delta^{15}N$ values of bulk organic matter, and on environmental interpretation, from a lake sedimentary sequence by pre-analysis acid treatment methods. Quat. Sci. Rev. 30 (21−22), 3076–3087.
Brodie, C.R., Leng, M.J., Casford, J.S.L., Kendrick, C.P., Lloyd, J.M., Zong, Y.Q., Bird, M. I., 2011b. Evidence for bias in C and N concentrations and $\delta^{13}C$ composition of terrestrial and aquatic organic materials due to pre-analysis acid preparation methods. Chem. Geol. 282 (3–4), 67–83.
Brodribb, T.J., Feild, T.S., 2010. Leaf hydraulic evolution led a surge in leaf photosynthetic capacity during early angiosperm diversification. Ecol. Lett. 13 (2), 175–183.
Brongniart, A.T., 1837. Histoire des végétaux fossiles, ou, Recherches botaniques et géologiques sur les végétaux renfermés dans les diverses couches du globe. Tome 2. Landmarks II, monographs. G. Dufour et Ed. d'Ocagne, Paris, 72 pp.
Bruhn, D., Mikkelsen, T.N., Rolsted, M.M.M., Egsgaard, H., Ambus, P., 2014. Leaf surface wax is a source of plant methane formation under UV radiation and in the presence of oxygen. Plant Biol. 16 (2), 512–516.
Burnham, R.J., Spicer, R.A., 1986. Forest litter preserved by volcanic activity at El Chichon, Mexico: A potentially accurate record of the pre-eruption vegetation. Palaios 1, 158–161.
Bush, R.T., Wallace, J., Currano, E.D., Jacobs, B.F., McInerney, F.A., Dunn, R.E., Tabor, N.J., 2017. Cell anatomy and leaf $\delta^{13}C$ as proxies for shading and canopy structure in a Miocene forest from Ethiopia. Palaeogeogr. Palaeoclimatol. Palaeoecol. 485, 593–604.
Cavalcante, L.L., Barbolini, N., Bacsik, Z., Vajda, V., 2023. Analysis of fossil plant cuticles using vibrational spectroscopy: A new preparation protocol. Rev. Palaeobot. Palynol. 316, 104944.
Cavalier-Smith, T., 2005. Economy, speed and size matter: Evolutionary forces driving nuclear genome miniaturization and expansion. Ann. Bot. 95 (1), 147–175.
Cleal, C.J., Zodrow, E.L., 1989. Epidermal structure of some medullosan *Neuropteris* foliage from the middle and upper Carboniferous of Canada and Germany. Palaeontology 32, 837–882.
Colombi, C.E., Montañez, I.P., Parrish, J.T., 2011. Registro de la relación isotópica de carbono en la paleoflora de la Formación Ischigualasto (Triásico Superior), noroeste argentino: implicaciones paleoatmosféricas. Revista Brasileira de Paleontologia 14 (1), 39–50.
Colombi, C.E., Limarino, C.O., Alcober, O.A., 2017. Allogenic controls on the fluvial architecture and fossil preservation of the Upper Triassic Ischigualasto Formation, NW Argentina. Sediment. Geol. 362, 1–16.
Craine, J.M., Elmore, A.J., Aidar, M.P.M., Bustamante, M., Dawson, T.E., Hobbie, E.A., Kahmen, A., Mack, M.C., McLauchlan, K.K., Michelsen, A., Nardoto, G.B., Pardo, L. H., Peñuelas, J., Reich, P.B., Schuur, E.A.G., Stock, W.D., Templer, P.H., Virginia, R. A., Welker, J.M., Wright, I.J., 2009. Global patterns of foliar nitrogen isotopes and their relationships with climate, mycorrhizal fungi, foliar nutrient concentrations, and nitrogen availability. New Phytol. 183 (4), 980–992.
Cui, Y., Schubert, B.A., 2018. Towards determination of the source and magnitude of atmospheric CO_2 change across the early Paleogene hyperthermals. Glob. Planet. Chang. 170, 120–125.
Cúneo, N.R., Taylor, E.L., Taylor, T.N., Krings, M., 2003. In situ fossil forest from the upper Fremouw Formation (Triassic) of Antarctica: paleoenvironmental setting and paleoclimate analysis. Palaeogeogr. Palaeoclimatol. Palaeoecol. 197 (3–4), 239–261.
Cutler, D.F., 1982. The Plant Cuticle. Academic Press, London, p. 461.
D'Angelo, J.A., 2019. Molecular structure of the cuticles of *Dicroidium* and *Johnstonia* (Corystospermaceae, Triassic, Argentina). Ecophysiological adaptations of two chemically indistinguishable, morphology-based taxa. Rev. Palaeobot. Palynol. 268, 109–124.
D'Angelo, J.A., 2023. Chemotaxonomy, biomechanics, and paleophysiology of *Alethopteris ambigua* and *Neuropteris ovata* var. simonii (late Pennsylvanian, Canada). A chemometric approach. Int. J. Coal Geol. 273, 104263.
D'Angelo, J.A., Zodrow, E.L., 2011. Chemometric study of functional groups in different layers of *Trigonocarpus grandis* ovules (Pennsylvanian seed fern, Canada). Org. Geochem. 42 (9), 1039–1054.
D'Angelo, J.A., Zodrow, E.L., 2018. Density and biomechanical properties of fossil fronds. A case study of *Neuropteris ovata* (seed fern, late Pennsylvanian, Canada). Int. J. Coal Geol. 198, 63–76.
D'Angelo, J.A., Zodrow, E.L., 2022. Chemotaxonomic comparison of the seed ferns *Odontopteris cantabrica* and *Odontopteris schlotheimii*, Middle Pennsylvanian Sydney Coalfield, Canada. Lethaia 55 (2), 1–8.
D'Angelo, J.A., Diaz, M.A.L., Fueyo, G.M.D., 2024a. Sweet or bitter? Preliminary data on the biomechanics, physiology, and possible nutritional quality of cretaceous gymnosperms leaves (Patagonia, Argentina). Rev. Palaeobot. Palynol. 326, 105129.
D'Angelo, J.A., Hower, J.C., Camí, G., 2024b. Fossil cutin of *Karinopteris* (Middle Pennsylvanian pteridosperm) from the "paper" coal of Indiana, USA. Int. J. Coal Geol. 284, 104460.
Dawson, T.E., Mambelli, S., Plamboeck, A.H., Templer, P.H., Tu, K.P., 2002. Stable isotopes in plant ecology. Annu. Rev. Ecol. Syst. 33 (1), 507–559.
de Leeuw, J.W., Versteegh, G.J.M., van Bergen, P.F., 2006. Biomacromolecules of algae and plants and their fossil analogues. Plant Ecol. 182 (1–2), 209–233.
DeNiro, M.J., Epstein, S., 1977. Mechanism of carbon isotope fractionation associated with lipid synthesis. Science 197 (4300), 261–263.
Diaz, M.A.L., D'Angelo, J.A., Del Fueyo, G.M., Zodrow, E.L., 2018. Fossilization Model for *Squamastrobus Tigrensis* foliage in a volcanic-ash deposit: implications for preservation and taphonomy (Podocarpaceae, lower cretaceous, Argentina). Palaios 33 (7), 323–337.
Diefendorf, A.F., Freimuth, E.J., 2017. Extracting the most from terrestrial plant-derived *n*-alkyl lipids and their carbon isotopes from the sedimentary record: A review. Org. Geochem. 103, 1–21.
Diefendorf, A.F., Mueller, K.E., Wing, S.L., Koch, P.L., Freeman, K.H., 2010. Global patterns in leaf ^{13}C discrimination and implications for studies of past and future climate. Proc. Natl. Acad. Sci. USA 107 (13), 5738–5743.
Dilcher, D.L., 1974. Approaches to the identification of angiosperm leaf remains. Bot. Rev. 40 (1), 1–157.
Drovandi, J.M., Correa, G.A., Colombi, C.E., Césari, S.N., 2022. (Szajnocha) Archangelsky from exceptional Carnian leaf litters of the Ischigualasto Formation, westernmost Gondwana. Hist. Biol. 34 (7), 1260–1273.
Esau, K., 1977. Anatomy of Seed Plants. John Wiley and Sons, New York, p. 550.
Faizullah, L., Morton, J.A., Hersch-Green, E.I., Walczyk, A.M., Leitch, A.R., Leitch, I.J., 2021. Exploring environmental selection on genome size in angiosperms. Trends Plant Sci. 26 (10), 1039–1049.
Farquhar, G.D., Sharkey, T.D., 1982. Stomatal conductance and photosynthesis. Annu. Rev. Plant Physiol. Plant Mol. Biol. 33, 317–345.
Farquhar, G.D., Caemmerer, S.V., Berry, J.A., 1980. A biochemical-model of photosynthetic CO_2 assimilation in leaves of C_3 species. Planta 149 (1), 78–90.
Farquhar, G.D., Ehleringer, J.R., Hubick, K.T., 1989. Carbon isotope discrimination and photosynthesis. Annu. Rev. Plant Physiol. Plant Mol. Biol. 40, 503–537.
Fay, C.A., 2014. Mid-Cretaceous pCO_2, Carbon-Cycling and the Rise of the Flowering Plants. Ph.D. Thesis,. University College London.
Feild, T.S., Sage, T.L., Czerniak, C., Iles, W.J.D., 2005. Hydathodal leaf teeth of *Chloranthus japonicus* (Chloranthaceae) prevent guttation-induced flooding of the mesophyll. Plant Cell Environ. 28 (9), 1179–1190.
Ferguson, D.K., 1985. The origin of leaf-assemblages — new light on an old problem. Rev. Palaeobot. Palynol. 46 (1–2), 117–188.
Fisher, D.C., 1981. Crocodilian scatology, microvertebrate concentrations, and enamel-less teeth. Paleobiology 7 (2), 262–275.
Florin, R., 1951. Evolution in Cordaites and conifers. Acta Horti Bergiani 15, 285–388.
Florin, R., 1958. On Jurassic taxads and conifers from North-Western Europe and eastern Greenland. Acta Horti Bergiani 17, 257–402.
Franks, P.J., Royer, D.L., Beerling, D.J., Van de Water, P.K., Cantrill, D.J., Barbour, M.M., Berry, J.A., 2014. New constraints on atmospheric CO_2 concentration for the Phanerozoic. Geophys. Res. Lett. 41 (13), 4685–4694.
Fujisaki, W., Matsui, Y., Ueda, H., Sawaki, Y., Suzuki, K., Maruoka, T., 2022. Pre-treatment methods for accurate determination of total nitrogen and organic carbon contents and their stable Isotopic compositions: Re-evaluation from geological reference materials. Geostand. Geoanal. Res. 46 (1), 5–19.
Gastaldo, R.A., Demko, T.M., 2011. The relationship between continental landscape evolution and the plant-fossil record: Long term hydrologic controls on preservation.

In: Allison, P.A., Bottjer, D.J. (Eds.), Taphonomy. Aims & Scope Topics in Geobiology Book Series, Springer, Dordrecht, pp. 249–285.
Gastaldo, R.A., Huc, A.Y., 1992. Sediment facies, depositional environments, and distribution of phytoclasts in the recent Mahakam River delta, Kalimantan, Indonesia. Palaios 574–590.
Gitz, D.C., Baker, J.T., 2009. Methods for creating stomatal impressions directly onto archivable microscope slides. Agron. J. 101 (1), 232–236.
Göppert, H.R., 1841. Taxites scalariformis, eine neue Art fossilen Holzes. Archiv für Mineralogie und Geognosie 15, 727–730.
Gori, Y., Wehrens, R., Greule, M., Keppler, F., Ziller, L., La Porta, N., Camin, F., 2013. Carbon, hydrogen and oxygen stable isotope ratios of whole wood, cellulose and lignin methoxyl groups of Picea abies as climate proxies. Rapid Commun. Mass Spectrom. 27 (1), 265–275.
Graham, H.V., Patzkowsky, M.E., Wing, S.L., Parker, G.G., Fogel, M.L., Freeman, K.H., 2014. Isotopic characteristics of canopies in simulated leaf assemblages. Geochim. Cosmochim. Acta 144, 82–95.
Graham, H.V., Herrera, F., Jaramillo, C., Wing, S.L., Freeman, K.H., 2019. Canopy structure in late cretaceous and Paleocene forests as reconstructed from carbon isotope analyses of fossil leaves. Geology 47 (10), 977–981.
Greenwood, D.R., 1992. Taphonomic constraints on foliar physiognomie interpretations of late cretaceous and tertiary palaeoeclimates. Rev. Palaeobot. Palynol. 71 (1–4), 149–190.
Gröcke, D.R., 2020. Carbon isotope stratigraphy: Principles and applications. In: Montenari, M. (Ed.), Stratigraphy & Timescales. Academic Press, pp. 1–40.
Guignard, G., 2019. Thirty-three years (1986-2019) of fossil plant cuticle studies using transmission electron microscopy: A review. Rev. Palaeobot. Palynol. 271, 104097.
Guignard, G., 2021. Method for ultrastructural fine details of plant cuticles by transmission electron microscopy. Methodsx 8, 101391.
Guignard, G., Zhou, Z., 2005. Comparative studies of leaf cuticle ultrastructure between living and the oldest known fossil Ginkgos in China. Int. J. Plant Sci. 166 (1), 145–156.
Guignard, G., Carrizo, M.A., Diaz, M.A.L., Del Fueyo, G.M., 2024. TEM and EDS characterization in a Bennettitalean cuticle from the Lower Cretaceous Springhill Formation, Argentina. Rev. Palaeobot. Palynol. 320, 105005.
Gupta, N.S., 2014. Biopolymers: A molecular paleontology approach. In: Topics in Geobiology, 38. Springer, 1–174 pp.
Guy, R.D., Reid, D.M., 1986. Photosynthesis and the influence of CO_2-enrichment on $\delta^{13}C$ values in a C_3 halophyte. Plant Cell Environ. 9 (1), 65–72.
Guy, R.D., Fogel, M.F., Berry, J.A., Hoering, T.C., 1987. Isotope Fractionation during Oxygen Production and Consumption by Plants. In: Biggins, J. (Ed.), Progress in Photosynthesis Research. Springer, Dordrecht, pp. 597–600.
Hall, S.A., 1988. Prehistoric Vegetation and Environment at Chaco Canyon. Am. Antiq. 53 (3), 582–592.
Heredia, A., Benítez, J.J., Moreno, A.G., Domínguez, E., 2024. Revisiting plant cuticle biophysics. New Phytol. 244 (1), 65–73.
Heredia-Guerrero, J.A., Benítez, J.J., Domínguez, E., Bayer, I.S., Cingolani, R., Athanassiou, A., Heredia, A., 2014. Infrared and Raman spectroscopic features of plant cuticles: a review. Front. Plant Sci. 5, 305.
Holloway, P.T., 1982. Structure and histochemistry of plant cuticular membranes: an overview. In: Cutler, K.A.D.F., Price, C.E. (Eds.), The Plant Cuticle. Academic Press, London, pp. 1–32.
Holz, M., Simões, M.G., 2005. Taphonomy—overview of main concepts and applications to sequence stratigraphic analysis. In: Koutsoukos, E.A.M. (Ed.), Applied Stratigraphy. Springer, Dordrecht, pp. 249–278.
Jardine, P.E., Kent, M., Fraser, W.T., Lomax, B.H., 2019. Leaf cuticle chemistry across changing CO_2 regimes. Palz 93 (3), 549–558.
Jeffree, C.E., 1996. Structure and ontologeny of plant cuticles. In: Kersteins, G. (Ed.), Plant Cuticles, an Integrated and Functional Approach. Bios Scientific Publishers, Oxford, UK, pp. 33–82.
Jolliffe, J.B., Pilati, S., Moser, C., Lashbrooke, J.G., 2023. Beyond skin-deep: targeting the plant surface for crop improvement. J. Exp. Bot. 74 (21), 6468–6486.
Jordan, G.J., 2011. A critical framework for the assessment of biological palaeoproxies: predicting past climate and levels of atmospheric CO_2 from fossil leaves. New Phytol. 192 (1), 29–44.
Jordan, G.J., Carpenter, R.J., Brodribb, T.J., 2014. Using fossil leaves as evidence for open vegetation. Palaeogeogr. Palaeoclimatol. Palaeoecol. 395, 168–175.
Katsi, F., Kent, M.S., Jones, M., Fraserc, W.T., Jardine, P.E., Eastwood, W., Marianic, M., Osborne, C., Edwards, S., Lomax, B.H., 2024. FTIR spectra from grass pollen: A quest for species-level resolution of Poaceae and Cerealia-type pollen grains. Rev. Palaeobot. Palynol. 321.
Kerp, H., 1990. The study of fossil gymnosperms by means of cuticular analysis. Palaios 5 (6), 548–569.
Kerp, H., Krings, M., 1999. Light microscopy of fossil cuticles. In: Jones, T.P., Rowe, N.P. (Eds.), Fossil Plants and Spores: Modern Techniques. Geological Society of London, Bath, pp. 52–56.
Kipp, M.A., Stüeken, E.E., Strömberg, C.A.E., Brightly, W.H., Arbour, V.M., Erdei, B., Hill, R.S., Johnson, K.R., Kvacek, J., McElwain, J.C., Miller, I.M., Slodownik, M., Vajda, V., Buick, R., 2024. Nitrogen isotopes reveal independent origins of N-fixing symbiosis in extant cycad lineages. Nat. Ecol. Evol. 8 (1), 57–69.
Kohn, M.J., 2010. Carbon isotope compositions of terrestrial C_3 plants as indicators of (paleo)ecology and (paleo)climate. Proc. Natl. Acad. Sci. USA 107 (46), 19691–19695.
Kolattukudy, P.E., 1980. Bio-polyester membranes of plants - cutin and suberin. Science 208 (4447), 990–1000.
Kolattukudy, P.E., 1987. Lipid derived defensive polymers and waxes and their role in plant-microbe interaction. In: Stumpf, P.K. (Ed.), The Biochemistry of Plants. Academic Press, New York, pp. 291–314.
Kolattukudy, P.E., Espelie, K.E., 1989. Chemistry, biochemistry and function of suberin and associated waxes. In: Rowe, J. (Ed.), Natural Products of Woody Plants, Chemicals Extraneous to the Lignocellulosic Cell Wall. Springer, Berlin Heidelberg New York, pp. 304–367.
Kolattukudy, P.E., Fernandes, N.D., Azad, A.K., Fitzmaurice, A.M., Sirakova, T.D., 1997. Biochemistry and molecular genetics of cell-wall lipid biosynthesis in mycobacteria. Mol. Microbiol. 24 (2), 263–270.
Konrad, W., Roth-Nebelsick, A., Grein, M., 2008. Modelling of stomatal density response to atmospheric CO_2. J. Theor. Biol. 253 (4), 638–658.
Konrad, W., Katul, G., Roth-Nebelsick, A., Grein, M., 2017. A reduced order model to analytically infer atmospheric CO_2 concentration from stomatal and climate data. Adv. Water Resour. 104, 145–157.
Konrad, W., Royer, D.L., Franks, P.J., Roth-Nebelsick, A., 2021. Quantitative critique of leaf-based paleo-CO_2 proxies: Consequences for their reliability and applicability. Geol. J. 56 (2), 886–902.
Kouwenberg, L.L.R., McElwain, J.C., Kürschner, W.M., Wagner, F., Beerling, D.J., Mayle, F.E., Visscher, H., 2003. Stomatal frequency adjustment of four conifer species to historical changes in atmospheric CO_2. Am. J. Bot. 90 (4), 610–619.
Kouwenberg, L.L.R., Hines, R.R., McElwain, J.C., 2007. A new transfer technique to extract and process thin and fragmented fossil cuticle using polyester overlays. Rev. Palaeobot. Palynol. 145 (3–4), 243–248.
Kowalczyk, J.B., Royer, D.L., Miller, I.M., Anderson, C.W., Beerling, D.J., Franks, P.J., Grein, M., Konrad, W., Roth-Nebelsick, A., Bowring, S.A., Johnson, K.R., Ramezani, J., 2018. Multiple proxy estimates of atmospheric CO_2 from an early Paleocene rainforest. Paleoceanogr. Paleoclimatol. 33 (12), 1427–1438.
Kubínová, L., 1994. Recent stereological methods for measuring leaf anatomical characteristics: estimation of the number and sizes of stomata and mesophyll cells. J. Exp. Bot. 45 (270), 119–127.
Kumar, M.R., Singh, A., Kumar, N., Sarkar, D., 2015. Passive seismological imaging of the Narmada paleo-rift, Central India. Precambrian Res. 270, 155–164.
Kürschner, W.M., 1997. The anatomical diversity of recent and fossil leaves of the durmast oak (*Quercus petraea* Lieblein Q-pseudocastanea Goeppert) implications for their use as biosensors of palaeoatmospheric CO_2 levels. Rev. Palaeobot. Palynol. 96 (1–2), 1–30.
Laakso, K., Sullivan, J.H., Huttunen, S., 2000. The effects of UV-B radiation on epidermal anatomy in loblolly pine (*Pinus taeda* L.) and Scots pine (*Pinus sylvestris* L.). Plant Cell Environ. 23 (5), 461–472.
Lake, J.A., Woodward, F.I., 2008. Response of stomatal numbers to CO_2 and humidity: control by transpiration rate and abscisic acid. New Phytol. 179 (2), 397–404.
Liang, J.Q., Leng, Q., Höfig, D.F., Niu, G., Wang, L., Royer, D.L., Burke, K., Xiao, L., Zhang, Y.G., Yang, H., 2022a. Constraining conifer physiological parameters in leaf gas-exchange models for ancient CO_2 reconstruction. Glob. Planet. Chang. 209, 103737.
Liang, J.Q., Leng, Q., Xiao, L., Höfig, D.F., Royer, D.L., Zhang, Y.G., Yang, H., 2022b. Early Miocene redwood fossils from Inner Mongolia: CO_2 reconstructions and paleoclimate effects of a low Mongolian plateau. Rev. Palaeobot. Palynol. 305, 104743.
Lomax, B.H., Hilton, J., Bateman, R.M., Upchurch, G.R., Lake, J.A., Leitch, I.J., Cromwell, A., Knight, C.A., 2014. Reconstructing relative genome size of vascular plants through geological time. New Phytol. 201 (2), 636–644.
Loron, C.C., Dzul, E.R., Orr, P.J., Gromov, A.V., Fraser, N.C., McMahon, S., 2023. Molecular fingerprints resolve affinities of Rhynie chert organic fossils. Nat. Commun. 14 (1), 1387.
Lugardon, B., 1971. Contribution à la connaissance de la morphogenèse et de la structure des parois sporales chez les Filicinées isosporées. Ph.D. Thesis,. Universite' Paul Sabatier, Toulouse, 257 pp.
Lyons, P.C., Orem, W.H., Mastalerz, M., Zodrow, E.L., Viethredemann, A., Bustin, R.M., 1995. ^{13}C NMR, micro-FTIR and fluorescence-spectra, and pyrolysis-gas chromatograms of coalified foliage of late Carboniferous medullosan seed ferns, Nova Scotia, Canada: Implications for coalification and chemotaxonomy. Int. J. Coal Geol. 27 (2–4), 227–248.
Machesky, M.D., Sheldon, N.D., Hren, M.T., Smith, S.Y., 2025. The sensitivity of reconstructed carbon dioxide concentrations to stomatal preparation methods using a leaf gas exchange model. Appl. Plant Sci. 13 (1), e11629.
Maheshwari, H.K., Bajpai, U., 1996. Biochemical degradation of the cuticular membrane in an early cretaceous frond: A TEM study. Curr. Sci. 70 (10), 933–935.
Marcus, L.F., Berger, R., 1984. The significance of radiocarbon dates for Rancho La Brea. In: Martin, P.S., Klein, R.G. (Eds.), Quaternary Extinctions: A Prehistoric Revolution. University of Arizona Press, pp. 159–183.
Marshall, A.O., Marshall, C.P., 2015. Vibrational spectroscopy of fossils. Palaeontology 58 (2), 201–211.
Martin, G., Myers, D.A., Vogelmann, T.C., 1991. Characterization of plant epidermal lens effects by a surface replica technique. J. Exp. Bot. 42 (238), 581–587.
Martínez, L.C.A., Artabe, A.E., Archangelsky, S., 2020. Studies of the leaf cuticle fine structure of (Townrow) Artabe 1990 from Hoyada de Ischigualasto (Upper Triassic), San Juan Province, Argentina. Rev. Palaeobot. Palynol. 281.
Matthaeus, W.J., Schmidt, J., White, J.D., Zechmann, B., 2020. Novel perspectives on stomatal impressions: Rapid and non-invasive surface characterization of plant leaves by scanning electron microscopy. PLoS One 15 (9), e0238589.
Matthaeus, W.J., Macarewich, S.I., Richey, J., Montañez, I.P., McElwain, J.C., White, J. D., Wilson, J.P., Poulsen, C.J., 2023. A systems approach to understanding how plants transformed earth's environment in deep time. Annu. Rev. Earth Planet. Sci. 51, 551–580.

Maxbauer, D.P., Royer, D.L., LePage, B.A., 2014. High Arctic forests during the middle Eocene supported by moderate levels of atmospheric CO_2. Geology 42 (12), 1027–1030.
McElwain, J.C., Chaloner, W.G., 1996. The fossil cuticle as a skeletal record of environmental change. Palaios 11 (4), 376–388.
McElwain, J.C., Steinthorsdottir, M., 2017. Paleoecology, ploidy, paleoatmospheric composition, and developmental biology: A review of the multiple uses of fossil stomata. Plant Physiol. 174 (2), 650–664.
McElwain, J.C., Wade-Murphy, J., Hesselbo, S.P., 2005. Changes in carbon dioxide during an oceanic anoxic event linked to intrusion into Gondwana coals. Nature 435 (7041), 479–482.
McElwain, J.C., Yiotis, C., Lawson, T., 2015. Using modern plant trait relationships between observed and theoretical maximum stomatal conductance and vein density to examine patterns of plant macroevolution. New Phytol. 209 (1), 94–103.
McElwain, J.C., Montañez, I., White, J.D., Wilson, J.P., Yiotis, C., 2016. Was atmospheric CO_2 capped at 1000 ppm over the past 300 million years? Palaeogeogr. Palaeoclimatol. Palaeoecol. 441, 653–658.
McElwain, J.C., Matthaeus, W.J., Barbosa, C., Chondrogiannis, C., O' Dea, K., Jackson, B., Knetge, A.B., Kwasniewska, K., Nair, R., White, J.D., Wilson, J.P., Montañez, I.P., Buckley, Y.M., Belcher, C.M. and Nogué, S., 2024. Functional traits of fossil plants. New Phytol. 242 (2), 392–423.
Metcalfe, C.R., Chalk, L., 1979. Systematic Anatomy of Leaf and Stem, with a Brief History of the Subject. Anatomy of the Dicotyledons Second Edition, I. Clarendon Press, Oxford, p. 276.
Miller, S.E., 1983. Late quaternary insects of Rancho La Brea and McKittrick, California. Q. Res. 20 (1), 90–104.
Milligan, J.N., Royer, D.L., Franks, P.J., Upchurch, G.R., McKee, M.L., 2019. No evidence for a large atmospheric CO_2 spike across the Cretaceous-Paleogene boundary. Geophys. Res. Lett. 46 (6), 3462–3472.
Milligan, J.N., Flynn, A.G., Wagner, J.D., Kouwenberg, L.L.R., Barclay, R.S., Byars, B.W., Dunn, R.E., White, J.D., Zechmann, B., Peppe, D.J., 2021. Quantifying the effect of shade on cuticle morphology and carbon isotopes of sycamores: present and past. Am. J. Bot. 108 (12), 2435–2451.
Molina, I., Bueno, A., Heredia, A., Domínguez, E., 2023. Plant cuticle: from biosynthesis to ecological functions. Front. Plant Sci. 14, 1154255.
Montañez, I.P., McElwain, J.C., Poulsen, C.J., White, J.D., DiMichele, W.A., Wilson, J.P., Griggs, G., Hren, M.T., 2016. Climate, pCO_2 and terrestrial carbon cycle linkages during late Palaeozoic glacial-interglacial cycles. Nat. Geosci. 9 (11), 824–828.
Moreno, A.G., de Cózar, A., Prieto, P., Domínguez, E., Heredia, A., 2022. Radiationless mechanism of UV deactivation by cuticle phenolics in plants. Nat. Commun. 13 (1), 1786.
Moreno, A.G., Domínguez, E., Mayer, K., Xiao, N.N., Bock, P., Heredia, A., Gierlinger, N., 2023. 3D (x-y-t) Raman imaging of tomato fruit cuticle: Microchemistry during development. Plant Physiol. 191 (1), 219–232.
Mösle, B., Finch, P., Collinson, M.E., Scott, A.C., 1997. Comparison of modern and fossil plant cuticles by selective chemical extraction monitored by flash pyrolysis gas chromatography mass spectrometry and electron microscopy. J. Anal. Appl. Pyrolysis 40-41, 585–597.
Mösle, B., Collinson, M.E., Finch, P., Stankiewicz, B.A., Scott, A.C., Wilson, R., 1998. Factors influencing the preservation of plant cuticles: a comparison of morphology and chemical composition of modern and fossil examples. Org. Geochem. 29 (5–7), 1369–1380.
Murray, M., Soh, W.K., Yiotis, C., Batke, S., Parnell, A.C., Spicer, R.A., Lawson, T., Caballero, R., Wright, I.J., Purcell, C., McElwain, J.C., 2019. Convergence in maximum stomatal conductance of C_3 woody Angiosperms in natural ecosystems across bioclimatic zones. Front. Plant Sci. 10, 558.
Murray, M., Soh, W.K., Yiotis, C., Spicer, R.A., Lawson, T., McElwain, J.C., 2020. Consistent relationship between field-measured stomatal conductance and theoretical maximum stomatal conductance in C3 woody angiosperms in four major biomes. Int. J. Plant Sci. 181 (1), 142–154.
Nguyen Tu, T.T., Bocherens, H., Mariotti, A., Baudin, F., Pons, D., Broutin, J., Derenne, S., Largeau, C., 1999. Ecological distribution of Cenomanian terrestrial plants based on $^{13}C/^{12}C$ ratios. Palaeogeogr. Palaeoclimatol. Palaeoecol. 145 (1–3), 79–93.
Nguyen Tu, T.T., Derenne, S., Largeau, C., Mariotti, A., Bocherens, H., 2003. Comparison of leaf lipids from a fossil ginkgoalean plant and its extant counterpart at two degradation stages: diagenetic and chemotaxonomic implications. Rev. Palaeobot. Palynol. 124 (1–2), 63–78.
Nguyen Tu, T.T., Derenne, S., Largeau, C., Bardoux, G., Mariotti, A., 2004. Diagenesis effects on specific carbon isotope composition of plant *n*-alkanes. Org. Geochem. 35 (3), 317–329.
Nosova, N., Yakovleva, O., Ivanova, A., Kiritchkova, A., 2016. First data on the ultrastructure of the leaf cuticle of a Mesozoic conifer, Reymanowna (Miroviaceae). Rev. Palaeobot. Palynol. 233, 115–124.
O'Leary, M.H., 1981. Carbon isotope fractionation in plants. Phytochemistry 20 (4), 553–567.
Poole, I., Kürschner, W.M., 1999. Stomatal density and index: The practice. In: Jones, T. P., Rowe, N.P. (Eds.), Fossil Plants and Spores: Modern Techniques. Geological Society of London, Bath, pp. 257–260.
Poole, I., Weyers, J.D.B., Lawson, T., Raven, J.A., 1996. Variations in stomatal density and index: Implications for palaeoclimatic reconstructions. Plant Cell Environ. 19 (6), 705–712.
Poole, I., Lawson, T., Weyers, J.D.B., Raven, J.A., 2000. Effect of elevated CO_2 on the stomatal distribution and leaf physiology of *Alnus glutinosa*. New Phytol. 145 (3), 511–521.
Poorter, H., Pons, T.L., Reichgelt, T., 2025. Stomatal density and index are more responsive to light intensity than to $[CO_2]$: A meta-analysis and implications for paleo-CO_2 reconstruction. Plant Ecophysiol. 1 (1), 1.
Porter, A.S., Gerald, C.E.F., Yiotis, C., Montañez, I.P., McElwain, J.C., 2019. Testing the accuracy of new paleoatmospheric CO_2 proxies based on plant stable carbon isotopic composition and stomatal traits in a range of simulated paleoatmospheric O_2 :CO_2 ratios. Geochim. Cosmochim. Acta 259, 69–90.
Psenicka, J., Zodrow, E.L., Mastalerz, M., Bek, J., 2005. Functional groups of fossil marattialeans: chemotaxonomic implications for Pennsylvanian tree ferns and pteridophylls. Int. J. Coal Geol. 61 (3–4), 259–280.
Ravikumar, S., Surekha, R., Thavarajah, R., 2014. Mounting media: an overview. Journal of Dr. NTR Univ. Health Sci. 3, S1–S8.
Reichgelt, T., D'Andrea, W.J., 2019. Plant carbon assimilation rates in atmospheric CO_2 reconstructions. New Phytol. 223 (4), 1844–1855.
Reichgelt, T., D'Andrea, W.J., Fox, B.R.S., 2016. Abrupt plant physiological changes in southern New Zealand at the termination of the Mi-1 event reflect shifts in hydroclimate and pCO_2. Earth Planet. Sci. Lett. 455, 115–124.
Reichgelt, T., D'Andrea, W.J., Valdivia-McCarthy, A.D., Fox, B.R.S., Bannister, J.M., Conran, J.G., Lee, W.G., Lee, D.E., 2020. Elevated CO_2, increased leaf-level productivity, and water-use efficiency during the early Miocene. Clim. Past 16 (4), 1509–1521.
Reichgelt, T., Bannister, J.M., Lee, W.G., 2023. Leaf hydathode occurrence in indigenous New Zealand angiosperm trees: a preliminary survey. N. Z. J. Bot. 1–16.
Richey, J.D., Upchurch, G.R., Montañez, I.P., Lomax, B.H., Suarez, M.B., Crout, N.M.J., Joeckel, R.M., Ludvigson, G.A., Smith, J.J., 2018. Changes in CO_2 during Ocean Anoxic Event 1d indicate similarities to other carbon cycle perturbations. Earth Planet. Sci. Lett. 491, 172–182.
Richey, J.D., Montañez, I.P., White, J.D., DiMichele, W.A., Matthaeus, W.J., Poulsen, C. J., Macarewich, S.I., Looy, C.V., 2021. Modeled physiological mechanisms for observed changes in the late Paleozoic plant fossil record. Palaeogeogr. Palaeoclimatol. Palaeoecol. 562, 110056.
Richey, J.D., Nordt, L., White, J.D., Breecker, D.O., 2023. ISOORG23: an updated compilation of stable carbon isotope data of terrestrial organic materials for the Cenozoic and Mesozoic. Earth Sci. Rev. 241, 104439.
Roddy, A.B., Théroux-Rancourt, G., Abbo, T., Benedetti, J.W., Brodersen, C.R., Castro, M., Castro, S., Gilbride, A.B., Jensen, B., Jiang, G.F., Perkins, J.A., Perkins, S. D., Loureiro, J., Syed, Z., Thompson, R.A., Kuebbing, S.E., Simonin, K.A., 2020. The scaling of genome size and cell size limits maximum rates of photosynthesis with implications for ecological strategies. Int. J. Plant Sci. 181 (1), 75–87.
Roeske, C.A., O'leary, M.H., 1984. Carbon isotope effects on the enzyme-catalyzed carboxylation of ribulose bisphosphate. Biochemistry 23 (25), 6275–6284.
Rolfe, W.D.I., Durant, G.P., Fallick, A.E., Hall, A.J., Large, D.J., Scott, A.C., Smithson, T. R., Walkden, G.M., 1990. An early terrestrial biota preserved by Viséan vulcanicity in Scotland. In: Lockley, M.G., Rice, A. (Eds.), Volcanism and Fossil Biotas, Geological Society of America Special Paper, vol. 244, pp. 13–24.
Royer, D.L., 2001. Stomatal density and stomatal index as indicators of paleoatmospheric CO_2 concentration. Rev. Palaeobot. Palynol. 114 (1–2), 1–28.
Royer, D.L., Hren, M.T., 2017. Carbon isotopic fractionation between whole leaves and cuticle. Palaios 32 (4), 199–205.
Royer, D.L., Hren, M.T., 2022. Bulk carbon isotopic variability within leaves. Palaios 37 (8), 411–417.
Royer, D.L., Wing, S.L., Beerling, D.J., Jolley, D.W., Koch, P.L., Hickey, L.J., Berner, R.A., 2001. Paleobotanical evidence for near present-day levels of atmospheric CO_2 during part of the Tertiary. Science 292 (5525), 2310–2313.
Royer, D.L., Moynihan, K.M., McKee, M.L., Londoño, L., Franks, P.J., 2019. Sensitivity of a leaf gas-exchange model for estimating paleoatmospheric CO_2 concentration. Clim. Past 15 (2), 795–809.
Rozema, J., van de Staaij, J., Björn, L.O., Caldwell, M., 1997. UV-B as an environmental factor in plant life: stress and regulation. Trends Ecol. Evol. 12 (1), 22–28.
Sack, L., Melcher, P.J., Liu, W.H., Middleton, E., Pardee, T., 2006. How strong is intracanopy leaf plasticity in temperate deciduous trees? Am. J. Bot. 93 (6), 829–839.
Salisbury, E.J., 1928. On the causes and ecological significance of stomatal frequency, with special reference to the woodland flora. Philos. Trans. R. Soc. B 216, 1–65.
Sánchez, G.J., Contigiani, E.V., Coronel, M.B., Alzamora, S.M., García-Loredo, A., Nieto, A.B., 2021. Study of UV-C treatments on postharvest life of blueberries 'O'Neal' and correlation between structure and quality parameters. Heliyon 7 (6), e07190.
Scher, M.A., Barclay, R.S., Baczynski, A.A., Smith, B.A., Sappington, J., Bennett, L.A., Chakraborty, S., Wilson, J.P., Megonigal, J.P., Wing, S.L., 2022. The effect of CO_2 concentration on carbon isotope discrimination during photosynthesis in *Ginkgo biloba*: implications for reconstructing atmospheric CO_2 levels in the geologic past. Geochim. Cosmochim. Acta 337, 82–94.
Schlacher, T.A., Connolly, R.M., 2014. Effects of acid treatment on carbon and nitrogen stable isotope ratios in ecological samples: a review and synthesis. Methods Ecol. Evol. 5 (6), 541–550.
Schubert, B.A., Jahren, A.H., 2012. The effect of atmospheric CO_2 concentration on carbon isotope fractionation in C_3 land plants. Geochim. Cosmochim. Acta 96, 29–43.
Scoble, L., Ussher, S.J., Fitzsimons, M.F., Ansell, L., Craven, M., Fyfe, R.M., 2024. Optimisation of classification methods to differentiate morphologically-similar pollen grains from FT-IR spectra. Rev. Palaeobot. Palynol. 321, 105041.
Sheldon, N.D., Smith, S.Y., Stein, R., Ng, M., 2020. Carbon isotope ecology of gymnosperms and implications for paleoclimatic and paleoecological studies. Glob. Planet. Chang. 184, 103060.

Shi, G.L., Xie, Z.M., Li, H.M., 2014. High diversity of Lauraceae from the Oligocene of Ningming, South China. Palaeoworld 23 (3–4), 336–356.
Shi, G.L., Herrera, F., Herendeen, P.S., Leslie, A.B., Ichinnorov, N., Takahashi, M., Crane, P.R., 2018. Leaves of *Podozamites* and *Psedotorellia* from the early cretaceous of Mongolia: stomatal patterns and implications for relationships. J. Syst. Palaeontol. 16 (2), 111–137.
Slavík, B., 1974. Methods of Studying Plant Water Relationships. Ecological Studies. Acad. Publishing House of the Czechoslovak; Springer, Berlin, Heidelberg, Prague, p. 452.
Slodownik, M., Vajda, V., Steinthorsdottir, M., 2020. Fossil seed fern *Lepidopteris ottonis* from Sweden records increasing CO_2 concentration during the end-Triassic extinction event. Palaeogeogr. Palaeoclimatol. Palaeoecol. 564 (2021), 110157.
Spicer, R.A., 1989. Physiological characteristics of land plants in relation to environment through time. Earth Environ. Sci. Trans. R. Soc. Edinb. 80 (3–4), 321–329.
Spicer, R.A., 1991. Plant taphonomic processes. In: Allison, P.A., Briggs, D.E.G. (Eds.), Taphonomy: Releasing the Data Locked in the Fossil Record. Plenum Press, New York, pp. 71–113.
Stace, C.A., 1965a. Cuticular studies as an aid to plant taxonomy. Bull. Br. Museum (Natural History) Botany 4 (1), 1–78.
Stace, C.A., 1965b. The significance of the leaf epidermis in the taxonomy of the Combretaceae: I. A general review of tribal, generic and specific characters. Bot. J. Linn. Soc. 59 (378), 229–252.
Stace, C.A., 1966. The use of epidermal characters in phylogenetic considerations. New Phytol. 65, 304–318.
Stace, C.A., 1984. The taxonomic importance of the leaf surface. In: Heywood, V.H., Moore, D.M. (Eds.), Current Concepts in Plant Taxonomy. Academic Press, London, pp. 67–94.
Stein, R.A., Sheldon, N.D., Smith, S., 2019. Rapid response to anthropogenic climate change by *Thuja occidentalis*: implications for past climate reconstructions and future climate predictions. PeerJ 7, e7378.
Stein, R.A., Sheldon, N.D., Smith, S.Y., 2021a. C_3 plant carbon isotope discrimination does not respond to CO_2 concentration on decadal to centennial timescales. New Phytol. 229 (5), 2576–2585.
Stein, R.A., Sheldon, N.D., Smith, S.Y., 2021b. Pacific Northwest plants record multiannual atmosphere-Ocean circulation patterns. J. Geophys. Res. 126 (19) e2021JD035454.
Stein, R.A., Sheldon, N.D., Smith, S.Y., 2024. Comparing methodologies for stomatal analyses in the context of elevated modern CO_2. Life (Basel) 14 (1), 78.
Steinthorsdottir, M., Jardine, P.E., Rember, W.C., 2021. Near-future pCO_2 during the hot Miocene climatic optimum. Paleoceanogr. Paleoclimatol. 36 (1) e2020PA003900.
Sun, B.N., Yan, D.F., Xie, S.P., Wang, Y.D., 2009. 化石植物气孔与碳同位素的分析及应用 Analysis and Application of Stomata and Carbon Isotopes in Fossil Plants. Science Press, Beijing, p. 222.
Tareq, S.M., Kitagawa, H., Ohta, K., 2011. Lignin biomarker and isotopic records of paleovegetation and climate changes from Lake Erhai, Southwest China, since 18.5 ka BP. Quat. Int. 229 (1–2), 47–56.
Tichá, I., 1982. Photosynthetic characteristics during ontogenesis of leaves. 7. Stomata density and sizes. Photosynthetica 16 (3), 375–471.
Tieszen, L.L., 1991. Natural variations in the carbon isotope values of plants: Implications for archaeology, ecology, and paleoecology. J. Archaeol. Sci. 18 (3), 227–248.
Tipple, B.J., Pagani, M., 2007. The early origins of terrestrial C_4 photosynthesis. Annu. Rev. Earth Planet. Sci. 35, 435–461.
Uhl, D., Wuttke, M., Smith, K.T., Wedmann, S., Lehmann, T., 2024. Pre-Quaternary maar lakes/volcanogenic lakes as Konservat *Lagerstätten*—Messel and beyond. Palaeobiodiv. Palaeoenviron. 104, 753–761.
Unger, F., 1852. Iconographia plantarum fossilium. Denkschr Akad Wiss Math-Naturwiss Kl 4 (1), 71–118.
Upchurch, G.R., 1984. Cuticular anatomy of angiosperm leaves from the lower cretaceous Potomac Group. I. Zone I leaves. Am. J. Bot. 71 (2), 192–202.
Upchurch, G.R., 1995. Dispersed angiosperm cuticles: their history, preparation, and application to the rise of angiosperms in cretaceous and Paleocene coals, southern western interior of North America. Int. J. Coal Geol. 28 (2–4), 161–227.
Vaiglova, P., Snoeck, C., Nitsch, E., Bogaard, A., Lee-Thorp, J., 2014. Impact of contamination and pre-treatment on stable carbon and nitrogen isotopic composition of charred plant remains. Rapid Commun. Mass Spectrom. 28 (23), 2497–2510.
Vajda, V., Pucetaite, M., McLoughlin, S., Engdahl, A., Heimdal, J., Uvdal, P., 2017. Molecular signatures of fossil leaves provide unexpected new evidence for extinct plant relationships. Nat. Ecol. Evol. 1 (8), 1093–1099.
Vajda, V., Pucetaite, M., Steinthorsdottir, M., 2021. Geochemical fingerprints of Ginkgoales across the Triassic-Jurassic boundary of Greenland. Int. J. Plant Sci. 182 (7), 649–662.
van Bergen, P.F., Scott, A.C., Barrie, P.J., Deleeuw, J.W., Collinson, M.E., 1994. The chemical composition of Upper Carboniferous pteridosperm cuticles. Org. Geochem. 21 (1), 107–112.
van Bergen, F., Gale, J., Damen, K.J., Wildenborg, A.F.B., 2004. Worldwide selection of early opportunities for CO_2-enhanced oil recovery and CO_2-enhanced coal bed methane production. Energy 29 (9–10), 1611–1621.
Van Devender, T.R., Thompson, R.S., Betancourt, J.L., 1987. Vegetation history of the deserts of southwestern North America; The nature and timing of the Late Wisconsin-Holocene transition. In: Ruddiman, W.F., Wright, H.E.J. (Eds.), North America and Adjacent Oceans During the Last Deglaciation. Geological Society of America, pp. 323–352.
van Roij, L., Sluijs, A., Laks, J.J., Reichart, G.J., 2017. Stable carbon isotope analyses of nanogram quantities of particulate organic carbon (pollen) with laser ablation nano combustion gas chromatography/isotope ratio mass spectrometry. Rapid Commun. Mass Spectrom. 31 (1), 47–58.
Veselý, P., Bureš, P., Šmarda, P., Pavlíček, T., 2012. Genome size and DNA base composition of geophytes: the mirror of phenology and ecology? Ann. Bot. 109 (1), 65–75.
Walton, J., 1935. Scottish lower Carboniferous plants: the fossil hollow trees of Arran and their branches (*Lepidophloios wünschianus* Carruthers). Earth Environ. Sci. Trans. R. Soc. Edinb. 58 (2), 313–337.
Wang, Y., Guignard, G., Thevenard, F., Dilcher, D., Barale, G., Mosbrugger, V., Yang, X., Mei, S., 2005. Cuticular anatomy of *Sphenobaiera huangii* (Ginkgoales) from the Lower Jurassic of Hubei, China. American Journal of Botany 92 (4), 709–721.
Wang, J., Pfefferkorn, H.W., Zhang, Y., Feng, Z., 2012. Permian vegetational Pompeii from Inner Mongolia and its implications for landscape paleoecology and paleobiogeography of Cathaysia. Proc. Natl. Acad. Sci. USA 109 (13), 4927–4932.
Wellman, C.H., Axe, L., 1999. Extracting plant mesofossils and megafossils by bulk acid maceration. In: Jones, T.P., Rowe, N.P. (Eds.), Fossil Plants and Spores: Modern Techniques. Geological Society of London, Bath, pp. 11–14.
Weyers, J.D.B., Johansen, L.G., 1985. Accurate estimation of stomatal aperture from silicone-rubber impressions. New Phytol. 101 (1), 109–115.
Weyers, J.D.B., Lawson, T., 1997. Heterogeneity in stomatal characteristics. Adv. Bot. Res. 26, 317–352.
Weyers, J.D.B., Meidner, H., 1990. Methods in Stomatal Research. Longman Scientific & Technical, p. 233.
White, J.D., Montañez, I.P., Wilson, J.P., Poulsen, C.J., McElwain, J.C., DiMichele, W.A., Hren, M.T., Macarewich, S., Richey, J.D., Matthaeus, W.J., 2020. A process-based ecosystem model (paleo-bgc) to simulate the dynamic response of late carboniferous plants to elevated O_2 and aridification. Am. J. Sci. 320 (7), 547–598.
Whiteman, J.P., Smith, E.A.E., Besser, A.C., Newsome, S.D., 2019. A guide to using compound-specific stable isotope analysis to study the fates of molecules in organisms and ecosystems. Diversity 11 (1), 8.
Wilson, J.P., Montañes, I.P., White, J.D., DiMichele, W.A., McElwain, J.C., Poulsen, C.J., Hren, M.T., 2017. Dynamic Carboniferous tropical forests: new views of plant function and potential for physiological forcing of climate. New Phytol. 215 (4), 1333–1353.
Wing, S.L., 1988. Depositional environments of plant bearing sediments. In: DiMichele, W.A., Wing, S.L. (Eds.), Methods and Applications of Plant Paleoecology, The Paleontological Society Special Publication, vol. 3, pp. 1–13.
Wing, S.L., Hickey, L.J., Swisher, C.C., 1993. Implications of an exceptional fossil flora for late cretaceous vegetation. Nature 363 (6427), 342–344.
Witkowski, C.R., Leng, Q., Reid, C.W., Feng, L., Yang, H., 2022. Tissue decay tested in modern *Metasequoia* leaves: Implications for early diagenesis of leaves in fossil *Lagerstätten*. Rev. Palaeobot. Palynol. 304, 104720.
Wu, S.C., Zhao, B.Y., 2017. Using clear nail polish to make *Arabidopsis* epidermal impressions for measuring the change of stomatal aperture size in immune response. In: Shan, L., He, P. (Eds.), Plant Pattern Recognition Receptors. Humana Press, Methods in Molecular Biology. Methods in Molecular Biology, pp. 243–248.
Yang, X.J., Guignard, G., Thevenard, F., Wang, Y.D., Barale, G., 2009. Leaf cuticle ultrastructure of *Pseudofrenelopsis dalatzensis* (Chow et Tsao) Cao ex Zhou (Cheirolepidiaceae) from the lower cretaceous Dalazi Formation of Jilin, China. Review of Palaeobotany and Palynology 153 (1–2), 8–18.
Zahajská, P., Cepicková, J., Trubac, J., Pedentchouk, N., Kvacek, J., 2024. The relationship of plant leaf $\delta^{13}C_{n\text{-alkanes}}$ and salinity in coastal ecosystems applied to palaeobotany: Case study from the Cenomanian of the Bohemian Cretaceous Basin, Czechia. Palaeogeography Palaeoclimatology Palaeoecology 638, 112052.
Zhang, X.Q., Wang, Y.D., Dilcher, D.L., Manchester, S.R., 2020. *Wireroadia*, a new genus of winged fruit from the cretaceous of Alabama and New England, USA. Int. J. Plant Sci. 181 (9), 898–910.
Zhang, X.Q., Royer, D.L., Shi, G.L., Ichinnorov, N., Herendeen, P.S., Crane, P.R., Herrera, F., 2024. Estimates of late early cretaceous atmospheric CO_2 from Mongolia based on stomatal and isotopic analysis of *Pseudotorellia*. Am. J. Bot. 111 (7), e16376.
Zhao, T., Wan, S., Li, S., Feng, Z., 2024. Leaf mining induced chemical defense of a late Triassic ginkgophyte plant. New Phytol. 245, 27–32.
Zodrow, E.L., 2021. The "fine chemical" structure of medullosalean cuticles and infrared spectroscopy. Rev. Palaeobot. Palynol. 287, 104383.
Zodrow, E.L., Mastalerz, M., 2001. Chemotaxonomy for naturally macerated tree-fern cuticles (Medullosales and Marattiales), Carboniferous Sydney and Mabou Sub-Basins, Nova Scotia, Canada. Int. J. Coal Geol. 47 (3–4), 255–275.
Zodrow, E.L., Mastalerz, M., 2007. Functional groups in a single pteridosperm species: Variability and circumscription (Pennsylvanian, Nova Scotia, Canada). Int. J. Coal Geol. 70 (4), 313–324.
Zodrow, E.L., Mastalerz, M., 2009. A proposed origin for fossilized Pennsylvanian plant cuticles by pyrite oxidation (Sydney Coalfield, Nova Scotia, Canada). Bull. Geosci. 84 (2), 227–240.
Zodrow, E.L., D'Angelo, J.A., Mastalerz, M., Keefe, D., 2009. Compression-cuticle relationship of seed ferns: Insights from liquid-solid states FTIR (late Palaeozoic-early Mesozoic, Canada-Spain-Argentina). Int. J. Coal Geol. 79 (3), 61–73.
Zodrow, E.L., Mastalerz, M., Werner-Zwanziger, U., D'Angelo, J.A., 2010. Medullosalean fusain trunk from the roof rocks of a coal seam: Insight from FTIR and NMR (Pennsylvanian Sydney Coalfield, Canada). Int. J. Coal Geol. 82 (1–2), 116–124.
Zodrow, E.L., Mastalerz, M., Helleur, R., 2012. *Lepidodendron dawsonii*: functional groups and pyrolysates of compression and fossilized-cuticle (late Asturian, Canada). Geologia Croatica 65 (3), 367–374.